DNA damage induces a kinetochore-based ATM/ATR-independent SAC arrest unique to the first meiotic division in mouse oocytes.

Simon I.R. Lane[1,*], Stephanie L. Morgan[1], Tianyu Wu[1], Josie K. Collins[1], Julie A. Merriman[1], Elias Ellnati[2], James M. Turner[2] & Keith T. Jones[1,*]

1. Biological Sciences, Faculty of Natural and Environmental Sciences, University of Southampton, Southampton, SO17 1BJ,
2 The Francis Crick Institute, London, NW1 1AT, UK.

*Correspondence should be addressed to either KTJ or SIRL, Biological Sciences, Faculty of Natural and Environmental Sciences, University of Southampton, Southampton SO17 1BJ, UK.
Tel: +44 (0)23 8059 3349
Email: KTJ, K.T.Jones@soton.ac.uk SIRL, Simon.Lane@soton.ac.uk;

Key words: Chromosomes, DNA Damage Response; Etoposide; Oocyte; Meiosis; Spindle Assembly Checkpoint.

Summary statement

Fully grown mouse oocytes in response to DNA damage will abruptly stop their first meiotic division. This is due to activation of the Spindle Assembly Checkpoint.

Abstract

Mouse oocytes carrying DNA damage arrest in meiosis I, thereby preventing creation of embryos with deleterious mutations. The arrest is dependent on the spindle assembly checkpoint, which results in anaphase-promoting complex (APC) inhibition. However, little is understood about how this checkpoint is engaged following DNA damage. Here, we find that within minutes DNA damage assembles checkpoint proteins at the kinetochore, not at damage sites along chromosome arms, such that the APC is fully inhibited within 30 min. Despite this robust response, there is no measurable loss in k-fibres, or tension across the bivalent. Through pharmacological inhibition we observed the response is dependent on Mps1 kinase, Aurora kinase, and haspin. Using oocyte specific knockouts we find the response does not require the DNA damage response kinases ATM or ATR. Furthermore, checkpoint activation does not occur in response to DNA damage in fully mature eggs during meiosis II, despite the divisions being separated by just a few hours. Therefore, mouse oocytes have a unique ability to sense DNA damage rapidly by activating the checkpoint at their kinetochores.

Introduction

The spindle assembly checkpoint (SAC) plays an essential role in reducing chromosome segregation errors by coupling anaphase-onset with biorientation, a state in which sister kinetochores are attached to microtubules emanating from opposite spindle poles (Foley and Kapoor, 2013; Lara-Gonzalez et al., 2012). Current models suggest unattached kinetochores bind Mad1 protein, along with Mad2 to form a platform on which a conformational activation of a further recruited Mad2 can take place (Kulukian et al., 2009; Zhou et al., 2016). Activated Mad2 is then released into the cytoplasm to form a powerful inhibitor of the Anaphase Promoting Complex (APC), known as the Mitotic Checkpoint Complex (MCC) (De Antoni et al., 2005; Izawa and Pines, 2015; Kulukian et al., 2009). When chromosomes biorientate, Mad1 along with Mad2 is displaced from kinetochores. This leads to APC activation, through loss of MCC, and so B-type cyclin and securin degradation; these events are essential for mitotic exit (Foley and Kapoor, 2013; Lara-Gonzalez et al., 2012).

There is much interest in how the SAC is controlled during meiosis I (MI) in mammalian oocytes because of the high rates of mis-segregation of the paired homologous chromosomes (bivalents) during this division (Jones and Lane, 2013; Nagaoka et al., 2012; Touati and Wassmann, 2016). Such mis-segregation leads to early embryo loss, birth defects, and infertility. Despite these errors, the SAC is present and active in mouse oocytes since loss or knockdown of its components increases rates of bivalent mis-segregation (Hached et al., 2011; Homer et al., 2005; Li et al., 2009; Niault et al., 2007; Touati et al., 2015; Zhang et al., 2005). However, although present, the SAC appears unable to respond to small numbers of non-biorientated bivalents (Gui and Homer, 2012; Hached et al., 2011; Jones and Lane, 2013; Kolano et al., 2012; Lane et al., 2012; Nagaoka et al., 2011). The reason why the meiotic SAC appears insensitive to a small number of errors is unclear, but may be related to the unique architecture of MI. It is a division of bivalents generating sister chromatid pairs with a single fused sister kinetochore achieving monopolar attachment.

The female meiotic SAC in oocytes is also activated by DNA damage associated with double strand breaks (DSBs) (Collins et al., 2015; Marangos et al., 2015). In these studies both chemical (etoposide, bleomycin, phleomycin, doxorubicin) and physical (ionising radiation, UVB) agents caused a metaphase arrest that was dependent on SAC activity. This contrasts with DNA damage induced during mitosis in somatic cells, which although leading to segregation errors, is not associated with any capacity to activate the SAC and arrest cells (Bakhoum et al., 2014; Cesare, 2014; Giunta et al., 2010; Orthwein et al., 2014; Terasawa et al., 2014).

Here we have studied the relationship between the canonical SAC, influenced by kinetochore microtubule attachment, and the DNA damage response (DDR) induced SAC in mouse oocytes using 4D-CLSM microscopy, pharmacological inhibitors and knockout mice. We find that the MI oocyte is uniquely sensitive to DNA damage, as arrest is not seen in MII eggs. This arrest does not require ATM or ATM kinases, and does not require a loss of tension or attachment between kinetochores and microtubules. Further, we demonstrate the signal comes from kinetochores/centromeres and not chromosome arms.

Results

Inhibition of APC activity associated with DNA damage in oocytes

DNA damage that occurs in fully-grown Germinal Vesicle stage oocytes immediately prior to nuclear envelope breakdown (NEB) causes an arrest several hours later in MI that is dependent on the SAC (Collins et al., 2015; Marangos et al., 2015). As such the arrest is ameliorated by Mad2 knockdown, expression of a dominant negative Bub1, or by inhibition of Mps1 kinase activity. Here we wanted to examine this association of DNA damage with SAC activation in more detail, and this was done by inducing DNA damage after NEB. This later addition of DNA damaging agents allows the initiating event of DNA damage to be studied at the same time that the APC is active, and allows measurement of the extent to which the SAC is reactivated.

Initially we wanted to determine how soon after DNA damage the SAC would be switched on sufficient to block APC activity. Oocytes expressing securin-YFP, as a real-time readout of APC activity, were imaged during addition of the canonical SAC activator nocodazole, or etoposide to induce DSBs. Oocytes were imaged between 6-7 h after NEB so as to record a measurable decline in securin levels, as a consequence of APC activity (Lane and Jones, 2014). As expected by its ability to depolymerise microtubules, nocodazole immediately diminished the rate of securin destruction and abolished it almost completely within a 10-15 min window (52.5 +/- 32.0 $\%h^{-1}$ to 1.1 +/- 9.2 $\%h^{-1}$, within 14 min; n=11; Fig 1A,B). Similarly etoposide also caused a substantial reduction in APC activity, although the rate of reduction was slower than with nocodazole (38.8 +/- 15.2 $\%h^{-1}$ to 1.3 +/- 10.3 $\%h^{-1}$, within 28 min; n=10; Fig 1A,B). Vehicle addition alone had no effect on securin degradation rate. Securin degradation first slowed significantly 6 min after nocodazole addition ($p=0.0119$, ANOVA), whereas following etoposide addition it took 14 min to achieve a significant reduction in the securin destruction rate ($p=0.0085$, ANOVA). This difference may reflect the indirect action of etoposide, which prevents repair of spontaneously generated DNA breaks. Most importantly however, the timings, illustrate the rapid response of the SAC to DNA damage in mouse oocytes, a process occurring over just a few minutes.

Timing of DNA damage induced recruitment of Mad1 to kinetochores

The above findings suggest that DNA damage has a capacity to activate the SAC sufficiently such that APC activity is inhibited over the course of several minutes. Therefore, one would anticipate seeing activation of upstream components of the SAC within this timeframe. Mad1-GFP was used as a dynamic probe of SAC activity during MI by microinjecting oocytes with its cRNA. In somatic cells Mad1 loading onto, and then removal from, kinetochores is an essential step in switching on, and off, the SAC respectively (Maldonado and Kapoor, 2011). Mad1-GFP has been used as a dynamic probe of SAC activity at kinetochores in a number of previous studies (Heinrich et al., 2014; Kruse et al., 2014; Matson and Stukenberg, 2014; Schweizer et al., 2013). In Mad1-expressing oocytes, an initial loading of this

SAC component onto sister kinetochore pairs was observed shortly after NEB (Fig 2A), and levels remained maximal for up to 3 h (Fig 2B). Between 3-7 h after NEB there was a continual decline in kinetochore-bound Mad1 until the time of anaphase (Fig 2A, 2B). As expected, this temporal profile of kinetochore-bound Mad1 correlates with APC activity, which begins to rise a few hours after NEB, and lasts for a period of ~3-4 h (Lane and Jones, 2014; Lane et al., 2012).

The SAC, once satisfied, can still be reactivated both in mitosis (Clute and Pines, 1999; Waters et al., 1998) and meiosis (Lane et al., 2012). This SAC reengagement could be observed as a significant rise in kinetochore-bound Mad1 following spindle disruption with nocodazole (Fig 2C), but not using a vehicle control (Supplementary Fig S1A and S1B). This was achieved quickly, within 5 min following addition of this spindle poison (6.1+/-14.4 arbitrary units at 0 min versus 43.1+/-37.0 arbitrary units at 5 min, $p<0.0001$, ANOVA, Fig 2D). The response to nocodazole was caused by activation of the SAC as kinetochore bound Mad1 was quickly dissipated following addition of reversine, an inhibitor of the essential checkpoint component Mps1 kinase (Supplementary Fig S1C and S1D).

To determine if DNA damage had the same temporal ability to recruit Mad1 onto kinetochores, the experiment was repeated with 40 µM etoposide, a dose effective at causing MI arrest (Collins et al., 2015). Similar to nocodazole, the checkpoint protein was observed to reload onto kinetochores (Fig 2E) reaching significantly raised levels at 15 min following drug addition (6.1+/-10.0 arbitrary units at 0 min versus 31.4+/-21.1 arbitrary units at 15 min, $p= 0.0055$, ANOVA, Fig 2F). Mad1 levels continued to rise over the course of the next 15 min towards a steady state high level.

Aurora, Haspin, and Mps1 kinase activity needed for DNA damage induced arrest

If DNA damage induced SAC activation, acting at the kinetochore, were similar in pathway to that induced by spindle depolymerisation then it should be dependent on Aurora and Mps1 kinases (Etemad and Kops, 2016;

Musacchio, 2015). Activities of both kinases can be reduced pharmacologically, and have been used to ameliorate SAC activity (Ditchfield et al., 2003; Hewitt et al., 2010; Lane and Jones, 2014). We employed the Aurora kinase inhibitor ZM447439 and the Mps1 inhibitor AZ3146, to block nocodazole induced Mad1 recruitment to kinetochores in oocytes (not shown), and then examined their effects on DNA damage following etoposide. Both the Mps1 kinase inhibitor (Fig 3A) and the Aurora kinase inhibitor (Fig 3B) were able to reverse the association of Mad1 with kinetochores, and this was rapid, being completed within 5 min of drug addition.

Haspin kinase (germ cell-specific gene 2 protein; GSG2) recruits to centromeres, by phosphorylation of histone H3, the Aurora kinase containing Chromosomal Passenger Complex (CPC) (Wang et al., 2010). Centromere localised Aurora kinase helps destabilise incorrect weak microtubule–kinetochore attachment, and is part of the SAC (Lara-Gonzalez et al., 2012; Musacchio, 2015). In mitosis, Aurora B associates with the CPC but in oocytes such association is primarily observed with its meiotic homologue Aurora C (Balboula and Schindler, 2014; Schindler et al., 2012). Interestingly this meiotic Aurora kinase is also found along chromosome arms and this localisation is blocked by 5-iodotubercidin (Balboula and Schindler, 2014; Nguyen et al., 2014; Quartuccio et al., 2017), a small-molecule inhibitor of haspin kinase (De Antoni et al., 2012; Wang et al., 2012). Inhibition of haspin kinase in oocytes is reported to reduce SAC activity (Quartuccio et al., 2017; Wang et al., 2016).

We added the haspin kinase inhibitor 5-Iodotubercidin to oocytes before an etoposide challenge, and as for ZM447439 and AZ3146, it also prevented Mad1 recruitment to kinetochores (Fig 4A, 4B). These data suggest that chromosome arm-localized Aurora C/CPC senses the DNA damage and communicates this signal to trigger the SAC response.

Mad1 and Cdc20 associate with kinetochores following DNA damage

Following etoposide induced DNA damage, recruitment of Mad1 appeared to be restricted to kinetochores rather than the chromatin between the

kinetochore pairs (Fig 2E). Such a finding is consistent with our previous observation that Mad2 kinetochore levels are also raised following DNA damage (Collins et al., 2015), and that the Mad1-Mad2 complex is being recruited specifically to kinetochores. However, it has recently been observed in *Drosophila* dividing neuroblast cells Cdc20, BubR1 and Bub3, but not Mad1 or Mad2, accumulate on chromosome arms following DNA damage (Derive et al., 2015). It may therefore be that some components of the SAC can be recruited to sites of DNA damage on chromosome arms while others are not. Hence here we compared Cdc20 and Mad1 localisation to determine if any association with DNA could be visualised with either the canonical SAC activator nocodazole, compared with etoposide 60 min after treatment. Following nocodazole, as expected recruitment of Mad1 (Fig 5A) and Cdc20 (Fig 5B) was confined to the two telocentric sister kinetochore pairs. Identical patterns of recruitment of Mad1 and Cdc20 were also observed following DNA damage (Fig 5C,D). As a further precaution we exposed oocytes expressing Mad1-GFP to etoposide for 15 minutes, a dose 10x higher than that used above. There was still no recruitment of GFP to the chromosome arms above background levels (Fig S2). Therefore, no evidence was found for any Mad1 or Cdc20 localisation along the chromosome arms. If it does happen it is at a level not significantly above the background fluorescence, and is certainly far below the level of accumulation at kinetochores.

DNA damage does not dissipate k-fibres or reduce bivalent stretch

In the canonical SAC pathway the checkpoint responds to vacant kinetochores, using them as a template to generate MCC (Foley and Kapoor, 2013; Kulukian et al., 2009; Lara-Gonzalez et al., 2012; Musacchio, 2015). Therefore, kinetochore attachment to microtubules was tested following DNA damage by measuring the percentage of end-on microtubule attached kinetochores (k-fibres). They are associated with loss of SAC activity in mouse oocytes during MI (Lane et al., 2012; Rattani et al., 2013) and can be distinguished by their stability at cold temperatures (Amaro et al., 2010; Salmon and Segall, 1980; Toso et al., 2009). Therefore following cold treatment and fixation, each kinetochore pair of a bivalent was assessed as being attached or unattached to k-fibres (Fig 6A). In total 44 oocytes at 7 h

after NEB were imaged, with 1357/1760 (77.1%) kinetochores being successfully scored as attached or non-attached. In vehicle controls, the vast majority of kinetochores were associated with k-fibres (90.2%, n=650: Fig 6B). Nocodazole, because it depolymerises tubulin, was very effective at severely reducing k-fibre number (0.3%, n=344; Fig 6B), but in contrast etoposide had no effect (92.6%, n=363; Fig 6B). These data suggest the SAC is not being triggered by conspicuous k-fibre loss following DNA damage.

Tension generated across the kinetochore, in addition to k-fibre attachment, plays a role in switching off the SAC (Maresca and Salmon, 2009; Santaguida et al., 2011; Uchida et al., 2009). Tension development leading to stretch is propagated differently in MI, compared to meiosis II and mitosis, because of the paired sister kinetochores and the structure of the bivalent (see Discussion). However, tension across the bivalent can be measured in two ways: (i) by the stretch across the length of the bivalent, or inter-homolog kinetochore stretch (ihK-K stretch), which would develop when amphitelic k-fibre attachment provides tension, and (ii) centromeric-kinetochore stretch (C-K stretch), which would develop as the kinetochore based k-fibre pulls on the centromere at one pole. To measure ihK-K and C-K stretch we over-expressed the outer-kinetochore protein Spc24 coupled to mCherry and a TALE protein that recognises the major satellite repeat (pericentromeric region) coupled to mClover (Fig 6C). Spc24 is a kinetochore based protein in mouse oocytes, as in all other cells, and is essential for correct bivalent segregation (Zhang et al., 2016), while the TALE construct has been used previously to label major satellite repeats in live mouse cells (Thanisch et al., 2014). Both measures of bivalent stretch were reduced when oocytes were treated with monastrol, showing biorientated bivalents decrease in length by ~twofold when k-fibre tension is lost (Fig 6D), and that stretch between the centromere and the sister kinetochore pair is significantly reduced (Fig 6E). However treatment with etoposide had no effect on either of these measures of tension (Fig 6D,E). Therefore, taken together in terms of the usual factors known to influence SAC activity and satisfaction, namely attachment and tension, no significant changes can be observed following DNA damage.

ATM/ATR are not involved in DNA damaged induced arrest

The canonical sensing of DNA damage involves either ataxia telangiectasia-mutated (ATM), or ATM and Rad3-related (ATR), which are phosphoinositide 3-kinase-related kinases (PIKKs) (Awasthi et al., 2015; Sirbu and Cortez, 2013). These two kinases are directly recruited to the site of DNA damage where they signal the process of repair (Caron et al., 2015; Falck et al., 2005; Nakada et al., 2003). Additionally, these PIKKs have also been implicated in the SAC, either interacting directly with specific SAC components or being involved in overall SAC efficacy (Dotiwala et al., 2010; Eliezer et al., 2014; Kim and Burke, 2008; Lawrence et al., 2015; Yang et al., 2014). However, a pharmacological ATM inhibitor failed to affect oocyte arrest when used previously on DNA damaged suggesting that instead ATR may be more important here (Marangos et al., 2015). Therefore, it was important to examine if ATM and ATR acting together were essential in transducing the DNA damage signal to the SAC.

Doses of inhibitors of ATM (KU55933) and ATR (ATR kinase inhibitor II), were used to inhibit γ-H2AX (Histone 2AX phosphorylated on serine 139) staining, a marker of DNA double strand breaks, following addition of etoposide (Fig 7A,B, Supplementary Fig S3). Both PIKKs are involved in this process. Maturing oocytes in the presence of these PIKK inhibitors had no negative affect on their ability to complete MI. However, they failed to block the effects of etoposide on arrest (Fig 7C). To confirm the lack of involvement of both ATM and ATR in the ability of DNA damage to cause SAC mediated arrest, conditional double knockout mice were used. A conditional oocyte specific knockout of these PIKKs was generated using mice with floxed genes for both *Atm* and *Atr*, mated to mice with *Cre* expression driven by the germ cell specific promoter *Ddx4*. Oocytes of the double knockout, ATM Δ/- ATR Δ/- for double knockout and ATM fl/- ATR fl/- for control, were then challenged with etoposide before NEB, and allowed to mature in vitro. It was observed that the loss of both PIKKs had no impact on the ability of etoposide to cause an MI arrest (Fig 7D), confirming the results from use of pharmacological inhibitors.

It is concluded therefore that ATM and ATR are not essential in the ability of DNA damage induced by etoposide to cause metaphase I arrest.

DNA damage to eggs does not block progression through meiosis II

In oocytes during MI, DNA damage induced by etoposide appears to cause activation of the SAC at the kinetochores. This contrasts with somatic cells during mitosis, which demonstrate little ability to arrest their cell cycle in M-phase following DNA damage. On completion of MI, oocytes have segregated their bivalents reductionally, and arrest spontaneously at metaphase II (metII). This second meiotic division (MII) involves equational division of pairs of sister chromatids, and thus resembles the division of chromosomes during mitosis (Clift and Schuh, 2013; Jones, 2011). We speculated whether these metII arrested oocytes, in their sensitivity to DNA damage, resemble somatic cells during mitosis or oocytes during MI.

Mad1-GFP and H2B-mCherry expressing metII eggs were challenged sequentially with etoposide and then nocodazole so as to measure the increase in kinetochore-bound Mad1 following DNA damage relative to spindle depolymerisation. To make direct comparison to MI oocytes, while imaging on the stage of the confocal microscope we co-cultured MI oocytes and metII eggs which could be exposed to drugs at the same time (Fig 8A,B). Following etoposide addition we observed that with respect to the MI oocytes (Fig 8A), metII eggs had a diminished response, attracting little Mad1 (Fig 8B). After 45 min of exposure to etoposide, nocodazole was added to remove microtubules and reveal the maximal Mad1 signal in the respective groups. Since MI oocytes have twice as many kinetochores as MII eggs we did not compare the absolute values, but rather normalised each group against their own maxima (15 min after nocodazole addition). This revealed that in response to etoposide the metII eggs recruited a minimal amount of Mad1, whereas MI oocytes recruited a significant amount of Mad1 (Fig 8C, $P<0.0001$, ANOVA with Tukey's multiple comparison test).

To determine if this lack of response of metII eggs translated into an ability to be activated and so complete MII following DNA damage, etoposide-treated eggs were incubated with Sr^{2+} containing medium. MetII eggs cultured in this

medium activated, because of its ability to induce changes in intracellular calcium that mimic sperm (Bos-Mikich et al., 1997; Carvacho et al., 2013); and such activation could be blocked by nocodazole (Fig 8D). This is predicted because physiological metII arrest is mediated by the APC inhibitor Emi2, but can also be induced by activation of the SAC (Madgwick et al., 2006; Tsurumi et al., 2004; Wu and Kornbluth, 2008).

DNA damage by itself did not cause any spontaneous egg activation, but critically DNA damaged eggs activated at a high rate in Sr^{2+} containing medium, at a level similar to eggs that were undamaged (Fig 8D). To rule out the possibility that the differential effect of etoposide induced DNA damage on meiotic arrest was due to the metII eggs having a lower permeability to etoposide, we used UVB irradiation. UVB (30 s exposure), like etoposide, is an effective activator of the SAC in meiosis I, causing MI arrest (Collins et al., 2015) (Figure S4A). MetII eggs treated with the same dose of UVB, activated at the same high rate as non-treated eggs (Fig S4).

These finding clearly demonstrate that metII eggs behave the same as somatic cells in mitosis, in terms of their inability to arrest in M-phase following DNA damage, and suggest it a unique feature of MI oocytes to activate the SAC and so arrest.

Discussion

Here it was discovered that DNA damage causes a rapid activation of the SAC during MI, allowing us to conduct an extensive examination of the mechanistic basis for this arrest. Previously it had been observed that DNA damage induced before NEB would lead to a MI arrest (Collins et al., 2015; Marangos et al., 2015). The present findings extend this to show that damage does not have to be historically induced, but rather it has the capacity to halt ongoing oocyte maturation within minutes.

We found many spatiotemporal similarities to canonical SAC activation induced for example with spindle poisons. Firstly, it was the kinetochore, rather than sites of DSBs along the chromosome arms, that acted as the

platform on which the SAC signal was generated. As such both Mad1 and Cdc20 were observed to be quickly recruited to kinetochores following etoposide addition, without any noticeable change elsewhere on bivalents. This extends the previous observation that Mad2, Bub1 and BubR1 are also present on kinetochores following prophase I damage (Collins et al., 2015; Marangos et al., 2015). It suggests that the MI arresting mechanism following damage are one and the same independent of when it is induced: before or after NEB. A conclusion which is supported by the observation that both are dependent on Mps1 kinase activity (Collins et al., 2015; Marangos et al., 2015). These findings collectively point to a mechanism of SAC activation that is similar to the attachment/tension sensing mechanism in prometaphase of somatic cells (Etemad and Kops, 2016; Foley and Kapoor, 2013; Lara-Gonzalez et al., 2012; Musacchio, 2015). A statement supported by the finding here that arrest appears sensitive to pharmacological Aurora kinase inhibition. Furthermore, the greater resolution imaging performed in the present study lends no evidence to the possibility that SAC component are localised along the chromosomes. Therefore, unlike in *Drosophila* dividing neuroblast cells we cannot image SAC proteins being recruited to the sites of DNA damage (Derive et al., 2015)

DNA induced damage did not cause SAC activation during meiosis II, despite the fact that the two meiotic divisions are separated by only a few hours. However, eggs, share the same property as somatic cells, which do not halt mitosis in response to damage, and instead respond in G1 by either repairing their DNA or undergoing apoptosis (Hustedt and Durocher, 2017). Therefore, on the basis of work presented here and what is known about the behaviour of somatic cells, it appears that DNA damage induced SAC activation is only observed in MI.

Here we give three possibilities for the sensitivity of the oocyte in MI to DNA damage. Firstly, that an MI specific protein(s) acts as a transducer, propagating a DNA damage response in the vicinity of the kinetochore into a SAC signal (Fig 9A). It may well prove that Aurora kinase C, which can be found on chromosome arms in meiosis I due to haspin kinase activity

(Quartuccio et al., 2017), is involved in this process. Here, haspin kinase inhibition, did block DNA damage induced Mad1 recruitment to kinetochores, and further work is needed to investigate this association. In support of its involvement is the loss of Aurora C from chromosome arms in MII (Sharif et al., 2010; Shuda et al., 2009), a period here marked with loss in the ability of DNA damage to cause meiotic arrest. Additionally, kinetochore and pericentromeric chromatin appear to overlap in MI (see Fig 6C), and other oocyte proteins do fulfill specific functions only in MI, such as meikin and EmiI (Kim et al., 2015; Marangos et al., 2007). Secondly, the unique chromatin architecture of the reductional division may endow the oocyte with sensitivity to DNA damage by virtue of the k-fibre pulling forces being spread across most of the length of the bivalent in MI (Fig 9B) so accentuating the tension sensing component of the SAC. However, this model is not preferred, as we did not detect any change in stretch across the bivalent or centromere following DNA damage. Therefore, if so, the reduction in tension does not translate into changes we can measure here. Thirdly, the sensitivity may be due to the unique structure of the co-segregating sister kinetochore pair in MI, which appears to allow both simultaneous k-fibre attachment and recruitment of SAC proteins (Brunet et al., 2003; Lane and Jones, 2014; Lane et al., 2012).

Historically we and others have thought of the SAC in oocytes as being weak or ineffectual at detecting errors in bivalent biorientation (Gui and Homer, 2012; Jones and Lane, 2013; Kolano et al., 2012; Lane et al., 2012; Nagaoka et al., 2011; Sebestova et al., 2012; Touati and Wassmann, 2016). This is because several misaligned bivalents have no impact on the timing of progression through MI (Lane et al., 2012). This clearly, if extrapolated to humans, would help explain the high rates of aneuploidy observed in human eggs and embryos. In contrast, no obvious morphometric changes are present in DNA damaged oocytes that go on to show a robust meiosis I arrest. As such it may be misplaced to describe the SAC as weak or ineffectual checkpoint in oocytes. It provides an effective checkpoint with respect to DNA damage, and can respond to levels of DNA damage present in endometriosis (Hamdan et al., 2016). We propose that the SAC sensitivity

to DNA damage comes as a result of the unique kinetochore or chromosome architecture of bivalents, likely involving meiosis specific proteins. We present clear evidence here using knockout mice, that it does not involve the ATM and ATR DNA damage pathway. The existence of such a response in oocytes in MI provides a mechanism by which the formation of DNA damaged embryos is prevented. It points to the SAC in meiosis being relevant to preventing not only whole chromosome aneuploidies but also the propagation of damaged chromatin.

Materials and Methods

All chemicals and reagents were from Sigma Aldrich (UK) unless otherwise stated.

Animals and Oocyte Culture. All mice were used in accordance with local and UK Home Office regulations on the use of animals in research. Three-to-four-week-old C57Bl6 female mice (Charles River, UK) were used. Germinal Vesicle stage oocytes were released from the ovaries of hormonally-primed females 44-52 h following 10 IU pregnant mares' serum gonadotrophin intraperitoneal injection (Centaur Services, UK). M2 medium supplemented with milrinone (1 µM) was used for collection to maintain prophase arrest (Yun et al., 2014). Oocytes were mechanically stripped from surrounding cells. For maturation, oocytes were washed into fresh M2 media and cultured usually for 14-16 h.

For metII eggs, female mice were superovulated by intraperitoneal injections of 10 IU pregnant mares' serum gonadotrophin, followed 48-52 h later by 10 IU human chorionic gonadotrophin (Centaur Services, UK). Cumulus oocyte complexes were collected 18 h later from the oviduct into M2 medium and briefly incubated in 300 IU ml^{-1} hyaluronidase (#H4272) to remove cumulus cells.

In some experiments oocytes and eggs were exposed to 300nm UV-B using a UV transilluminator (Hoefer Macrovue UV20; Fisher Scientific UK) for a 30 s incubation time (Collins et al., 2015).

Double knockout mice for *Atr* and *Atm*, generated on a mixed genetic background of 129/Sv and MF1 strains, were produced by mating *Atr* +/- *Atm* +/- *Cre tg/+* males with Atr flox/flox *Atm* flox/flox females. *Atm flox/flox* mice were obtained from the Jackson Laboratory, USA (strain 021444). The *Atm flox* allele contains two lox P sites flanking exons 57 and 58, which contain the core PIKK kinase domain of ATM. Cre-*lox* mediated recombination of the *Atm* flox allele leads to the removal of these essential kinase-domain encoding exons (Callen et al., 2009). *Atr flox/flox* mice were as described (Ruzankina et al., 2009).

Inhibitors

40 μM etoposide was added to oocytes for 15 min before NEB, or to maturing oocytes for times as indicated. 5-iodotubercidin (Cambridge Bioscience CAY10010375) was dissolved in 100% ethanol and diluted in media at 1:1000 to give a working concentration of 0.5 μM. Other additions were nocodazole (400 nM); ZM447439 (10 μM Bio-Techne, MN, USA), Mps1 inhibitor AZ3146 (2 μM, Bio-Techne), MG132 (10μM), KU55933 (10 μM, Merck-Millipore, UK), Bleomycin (1 μm, Abcam, UK) and ATR kinase inhibitor II (10 μM, Merck-Millipore, UK). All drugs were dissolved in DMSO and supplemented with the neutral detergent 200μg ml^{-1} pluronic acid to aid dispersion, and used at dilutions of 0.1% or below.

Parthenogenetic activation. Eggs were exposed to 0.1% DMSO, 40 μM etoposide or 400 nM nocodazole for 15 min. After washing, oocytes were either incubated in M2 for 6 h at 37 °C or Ca^{2+} free-M2 containing 10 mM $SrCl_2$ (#439665) and 5 μg ml^{-1} cytochalasin B to make them diploid (#C6762) for 2.5 h followed by M2 for 3.5 h. Oocytes treated with nocodazole were exposed throughout the 6 h activation. Oocytes were fixed as described below, stained briefly in DAPI and examined for evidence of pronuclei.

Kinetochore-microtubule attachment assay. Following 6 h maturation, oocytes were placed in ice cold M2 medium for 4 min, fixed for 15 min in PBS containing 2% formaldehyde and 0.05% Triton-X, and were then

permeabilised for 15 min in PBS containing 0.05% Triton-X (Lane et al., 2012). Fixing and permeabilising was performed at room temperature and oocytes were extensively washed with PBS between steps. Oocytes were incubated in a blocking buffer of 3% bovine serum albumin in PBS supplemented with Tween-20 and primary antibody for 1 h (ACA, Immunovision USA 1:400, #HCT-0100) (Lane et al., 2012). Following several washes oocytes were incubated with secondary antibody Alexafluor-555 (Life Technologies, UK, #A-21433, 1:500) and anti-α-tubulin-FITC (Sigma Aldrich UK, #F2168, 1:100) for 90 min. Antibody incubations were at 37°C in blocking solution. Oocytes were briefly counterstained with DAPI (10 µg ml^{-1}) to label chromatin before being mounted on glass slides with refractive index matched Citifluor (#CFMAF1-10, Citifluor Ltd, UK).

Homologue tension assay. Germinal Vesicle stage oocytes were microinjected with 500 and 600 ng $µl^{-1}$ mRNA encoding Spc24-mCherry and TALE Major Satellite-mClover (Maj.Sat.-mClover) respectively. Spc24-mCherry was made by PCR from testis cDNA and restriction enzyme cloning into pRN3 derivative plasmid with C-terminal mCherry. Maj.Sat.-mClover was a gift from Maria-Elena Torres-Padilla (Addgene plasmid # 47878) (Miyanari et al., 2013; Thanisch et al., 2014), and binds directly to the major satellite repeat DNA sequence. Oocytes were matured in M2 media to metaphase, 7 h after NEB, and then counterstained with Hoechst (20 µg ml^{-1}). Confocal image stacks were taken with a z-separation of 300 nm and X and Y pixel size of 0.036 µm. Images were processed in ImageJ (NIH, USA). A Gaussian blur (sigma = 2) was applied and the centre of mass of each signal was determined using an in-house macro that utilised the Foci_Picker3D Plugin (Version 1.0, CAS, China) (Du et al., 2011). Data were exported to Excel (Microsoft, USA) and distances between foci were calculated using 3D Pythagoras.

Immunofluorescence. Oocytes were fixed for 30 min in PHEM (PIPES, HEPES, EGTA, MgCl) buffer containing 2% formaldehyde and 0.05% Triton-X, and were then permeabilised for 15 min in PBS containing 1% PVP and 0.05% Triton-X. Fixing and permeabilising was performed at room

temperature and oocytes were extensively washed with PBS buffer between solutions. Oocytes were incubated at 4°C overnight in a blocking buffer of 7% goat serum in PBS supplemented with Tween-20 before primary antibody incubation (rabbit anti-γH2AX, Abcam, #ab11174, 1:200; or rabbit anti-Mad2, 1:1000, a kind gift from Dr R.H. Chen, Taipei, Taiwan; and ACA, 1:400, #HCT-0100, Immunovision USA). Following several washes oocytes were incubated with goat anti-rabbit Alexafluor 633 and anti-human Alexafluor-555 (Life Technologies, UK, 1:500, #a-21070). These incubations were at 37°C in blocking solution. Oocytes were briefly counterstained with Hoechst (20 µg ml^{-1}) to label chromatin before being mounted on glass slides with Citifluor (Citifluor Ltd, UK).

cRNA manufacture. cRNA was transcribed *in vitro* from purified linear dsDNA templates. T7 or T3 mMessage RNA polymerase kits (Ambion, Life Technologies, UK) were used for in vitro transcription reaction (Lane et al., 2012). cRNA was suspended in nuclease free water and the concentration of RNA products were determined by photospectroscopy.

Microinjection. Microinjections into oocytes were performed on the stage of an inverted TE300 microscope (Nikon, Japan), using micromanipulators (Narishige, Japan) and a 37°C heated chamber (Intracel, UK) (Yun et al., 2014). A single injection with a 0.1-0.3% volume was achieved using timed injection on a Pneumatic Picopump (World Precision Instruments, UK) and pipette RNA concentrations of 100-1200 ng $µl^{-1}$ (Lane et al., 2012; Yun et al., 2014).

Immunofluorescence imaging. All images were acquired using a Leica SP8 fitted with hybrid detectors and 63x oil immersion lens. Fluorochromes were imaged sequentially. When quantifying levels of γH2AX, a z-stack of the nuclear region was taken (~30 µm) and acquisition settings were not altered throughout the experiment. γH2AX staining was calculated as total nuclear fluorescence, on an 8-bit scale, following background subtraction from a

cytoplasmic region of equal area in the same oocyte. For the kinetochore-microtubule attachment assay, image stacks used a z resolution of 150 nm.

Time-lapse imaging. Timepoints were acquired at 2 or 5 min intervals using a Leica SP8 fitted with hybrid detectors, an environmental chamber set to 37°C, and a 63x oil immersion lens. Image stacks used a z resolution of 1.5 µm. In-lab software written in python programing language was used to image multiple stage regions and to track up to 30 oocytes in experiments using H2B and Mad1-2GFP to ensure chromosomes stayed in the centre of a ~26x26x24 µm imaging volume (Lane et al., 2017).

Image processing. Timelapse images from experiments with Mad1-2GFP were processed using ImageJ macros. The images were blurred (Gaussian blur, sigma=2) and background subtracted (subtraction of Gaussian blurred image, sigma = 10). The histone channel was then used to make a binary image which was dilated and used as a mask to filter out cytoplasmic Mad1 signals, leaving only Mad1 associated with the chromatin. A threshold was calculated such that two foci could be visualised on most bivalents at a suitable timepoint e.g. in prometaphase or after nocodazole addition. The 3D object counter plugin (Bolte and Cordelieres, 2006) was then used to measure the volume of Mad1 associated with chromatin at each timepoint using the pre-determined threshold.

Data Analysis. All images were processed using Image J (NIH, USA) with extended functionality provided by in-house macros (Lane and Jones, 2014; Yun et al., 2014). For securin-YFP time-lapse experiments, fluorescence intensities (arbitrary units on an 8-bit scale) were recorded in ImageJ and subsequently analysed in Microsoft Excel.

Statistical Analysis. Dichotomous data were analysed by Fisher's exact test. Sample means were compared using either a Student's t-test or Analysis of Variance, with a post-hoc test as stated. GraphPad Prism software (GraphPad Software, Inc) was used for all tests.

Acknowledgements

We thank Dr. Michael Lampson for the kind gift of Mad1-2GFP plasmid.

Competing interests

The authors declare no competing financial interests

Funding

This work was supported by the Biotechnology and Biological Sciences Research Council UK (BB/L006006/1 to K.T.J).

References

Amaro, A. C., Samora, C. P., Holtackers, R., Wang, E., Kingston, I. J., Alonso, M., Lampson, M., McAinsh, A. D. and Meraldi, P. (2010). Molecular control of kinetochore-microtubule dynamics and chromosome oscillations. *Nat Cell Biol* **12**, 319-329.

Awasthi, P., Foiani, M. and Kumar, A. (2015). ATM and ATR signaling at a glance. *J Cell Sci* **128**, 4255-4262.

Bakhoum, S. F., Kabeche, L., Murnane, J. P., Zaki, B. I. and Compton, D. A. (2014). DNA-damage response during mitosis induces whole-chromosome missegregation. *Cancer Discov* **4**, 1281-1289.

Balboula, A. Z. and Schindler, K. (2014). Selective disruption of aurora C kinase reveals distinct functions from aurora B kinase during meiosis in mouse oocytes. *PLoS genetics* **10**, e1004194.

Bolte, S. and Cordelieres, F. P. (2006). A guided tour into subcellular colocalization analysis in light microscopy. *J Microsc* **224**, 213-232.

Bos-Mikich, A., Whittingham, D. G. and Jones, K. T. (1997). Meiotic and mitotic Ca2+ oscillations affect cell composition in resulting blastocysts. *Dev Biol* **182**, 172-179.

Brunet, S., Pahlavan, G., Taylor, S. and Maro, B. (2003). Functionality of the spindle checkpoint during the first meiotic division of mammalian oocytes. *Reproduction* **126**, 443-450.

Callen, E., Jankovic, M., Wong, N., Zha, S., Chen, H. T., Difilippantonio, S., Di Virgilio, M., Heidkamp, G., Alt, F. W., Nussenzweig, A., et al. (2009). Essential role for DNA-PKcs in DNA double-strand break repair and apoptosis in ATM-deficient lymphocytes. *Mol Cell* **34**, 285-297.

Caron, P., Choudjaye, J., Clouaire, T., Bugler, B., Daburon, V., Aguirrebengoa, M., Mangeat, T., Iacovoni, J. S., Alvarez-Quilon, A., Cortes-Ledesma, F., et al. (2015). Non-redundant Functions of ATM and DNA-PKcs in Response to DNA Double-Strand Breaks. *Cell Rep* **13**, 1598-1609.

Carvacho, I., Lee, H. C., Fissore, R. A. and Clapham, D. E. (2013). TRPV3 channels mediate strontium-induced mouse-egg activation. *Cell Rep* **5**, 1375-1386.

Cesare, A. J. (2014). Mitosis, double strand break repair, and telomeres: A view from the end: How telomeres and the DNA damage response cooperate during mitosis to maintain genome stability. *BioEssays* **36**, 1054-1061.

Clift, D. and Schuh, M. (2013). Restarting life: fertilization and the transition from meiosis to mitosis. *Nat Rev Mol Cell Biol* **14**, 549-562.

Clute, P. and Pines, J. (1999). Temporal and spatial control of cyclin B1 destruction in metaphase. *Nat Cell Biol* **1**, 82-87.

Collins, J. K., Lane, S. I., Merriman, J. A. and Jones, K. T. (2015). DNA damage induces a meiotic arrest in mouse oocytes mediated by the spindle assembly checkpoint. *Nat Commun* **6**, 8553.

De Antoni, A., Maffini, S., Knapp, S., Musacchio, A. and Santaguida, S. (2012). A small-molecule inhibitor of Haspin alters the kinetochore functions of Aurora B. *The Journal of cell biology* **199**, 269-284.

De Antoni, A., Pearson, C. G., Cimini, D., Canman, J. C., Sala, V., Nezi, L., Mapelli, M., Sironi, L., Faretta, M., Salmon, E. D., et al. (2005). The Mad1/Mad2 complex as a template for Mad2 activation in the spindle assembly checkpoint. *Curr Biol* **15**, 214-225.

Derive, N., Landmann, C., Montembault, E., Claverie, M. C., Pierre-Elies, P., Goutte-Gattat, D., Founounou, N., McCusker, D. and Royou, A. (2015). Bub3-BubR1-dependent sequestration of Cdc20Fizzy at DNA breaks facilitates the correct segregation of broken chromosomes. *The Journal of cell biology* **211**, 517-532.

Ditchfield, C., Johnson, V. L., Tighe, A., Ellston, R., Haworth, C., Johnson, T., Mortlock, A., Keen, N. and Taylor, S. S. (2003). Aurora B couples chromosome alignment with anaphase by targeting BubR1, Mad2, and Cenp-E to kinetochores. *The Journal of cell biology* **161**, 267-280.

Dotiwala, F., Harrison, J. C., Jain, S., Sugawara, N. and Haber, J. E. (2010). Mad2 prolongs DNA damage checkpoint arrest caused by a double-strand break via a centromere-dependent mechanism. *Curr Biol* **20**, 328-332.

Du, G., Drexler, G. A., Friedland, W., Greubel, C., Hable, V., Krucken, R., Kugler, A., Tonelli, L., Friedl, A. A. and Dollinger, G. (2011). Spatial

dynamics of DNA damage response protein foci along the ion trajectory of high-LET particles. *Radiat Res* **176**, 706-715.

Eliezer, Y., Argaman, L., Kornowski, M., Roniger, M. and Goldberg, M. (2014). Interplay between the DNA damage proteins MDC1 and ATM in the regulation of the spindle assembly checkpoint. *J Biol Chem* **289**, 8182-8193.

Etemad, B. and Kops, G. J. (2016). Attachment issues: kinetochore transformations and spindle checkpoint silencing. *Curr Opin Cell Biol* **39**, 101-108.

Falck, J., Coates, J. and Jackson, S. P. (2005). Conserved modes of recruitment of ATM, ATR and DNA-PKcs to sites of DNA damage. *Nature* **434**, 605-611.

Foley, E. A. and Kapoor, T. M. (2013). Microtubule attachment and spindle assembly checkpoint signalling at the kinetochore. *Nat Rev Mol Cell Biol* **14**, 25-37.

Giunta, S., Belotserkovskaya, R. and Jackson, S. P. (2010). DNA damage signaling in response to double-strand breaks during mitosis. *The Journal of cell biology* **190**, 197-207.

Gui, L. and Homer, H. (2012). Spindle assembly checkpoint signalling is uncoupled from chromosomal position in mouse oocytes. *Development* **139**, 1941-1946.

Hached, K., Xie, S. Z., Buffin, E., Cladiere, D., Rachez, C., Sacras, M., Sorger, P. K. and Wassmann, K. (2011). Mps1 at kinetochores is essential for female mouse meiosis I. *Development* **138**, 2261-2271.

Hamdan, M., Jones, K. T., Cheong, Y. and Lane, S. I. (2016). The sensitivity of the DNA damage checkpoint prevents oocyte maturation in endometriosis. *Sci Rep* **6**, 36994.

Heinrich, S., Sewart, K., Windecker, H., Langegger, M., Schmidt, N., Hustedt, N. and Hauf, S. (2014). Mad1 contribution to spindle assembly checkpoint signalling goes beyond presenting Mad2 at kinetochores. *EMBO Rep* **15**, 291-298.

Hewitt, L., Tighe, A., Santaguida, S., White, A. M., Jones, C. D., Musacchio, A., Green, S. and Taylor, S. S. (2010). Sustained Mps1

activity is required in mitosis to recruit O-Mad2 to the Mad1-C-Mad2 core complex. *The Journal of cell biology* **190**, 25-34.

Homer, H. A., McDougall, A., Levasseur, M., Yallop, K., Murdoch, A. P. and Herbert, M. (2005). Mad2 prevents aneuploidy and premature proteolysis of cyclin B and securin during meiosis I in mouse oocytes. *Genes Dev* **19**, 202-207.

Hustedt, N. and Durocher, D. (2017). The control of DNA repair by the cell cycle. *Nat Cell Biol* **19**, 1-9.

Izawa, D. and Pines, J. (2015). The mitotic checkpoint complex binds a second CDC20 to inhibit active APC/C. *Nature* **517**, 631-634.

Jones, K. T. (2011). Anaphase-promoting complex control in female mouse meiosis. *Results Probl Cell Differ* **53**, 343-363.

Jones, K. T. and Lane, S. I. (2013). Molecular causes of aneuploidy in mammalian eggs. *Development* **140**, 3719-3730.

Kim, E. M. and Burke, D. J. (2008). DNA damage activates the SAC in an ATM/ATR-dependent manner, independently of the kinetochore. *PLoS genetics* **4**, e1000015.

Kim, J., Ishiguro, K., Nambu, A., Akiyoshi, B., Yokobayashi, S., Kagami, A., Ishiguro, T., Pendas, A. M., Takeda, N., Sakakibara, Y., et al. (2015). Meikin is a conserved regulator of meiosis-I-specific kinetochore function. *Nature* **517**, 466-471.

Kolano, A., Brunet, S., Silk, A. D., Cleveland, D. W. and Verlhac, M. H. (2012). Error-prone mammalian female meiosis from silencing the spindle assembly checkpoint without normal interkinetochore tension. *Proc Natl Acad Sci U S A* **109**, E1858-1867.

Kruse, T., Larsen, M. S., Sedgwick, G. G., Sigurdsson, J. O., Streicher, W., Olsen, J. V. and Nilsson, J. (2014). A direct role of Mad1 in the spindle assembly checkpoint beyond Mad2 kinetochore recruitment. *EMBO Rep* **15**, 282-290.

Kulukian, A., Han, J. S. and Cleveland, D. W. (2009). Unattached kinetochores catalyze production of an anaphase inhibitor that requires a Mad2 template to prime Cdc20 for BubR1 binding. *Dev Cell* **16**, 105-117.

Lane, S. I., Crouch, S. and Jones, K. T. (2017). Imaging chromosome separation in mouse oocytes by responsive 3D confocal timelapse microscopy. In *Meiosis* (ed. D. T. Stuart). New York: Humana Press.

Lane, S. I. and Jones, K. T. (2014). Non-canonical function of spindle assembly checkpoint proteins after APC activation reduces aneuploidy in mouse oocytes. *Nat Commun* **5**, 3444.

Lane, S. I., Yun, Y. and Jones, K. T. (2012). Timing of anaphase-promoting complex activation in mouse oocytes is predicted by microtubule-kinetochore attachment but not by bivalent alignment or tension. *Development* **139**, 1947-1955.

Lara-Gonzalez, P., Westhorpe, F. G. and Taylor, S. S. (2012). The spindle assembly checkpoint. *Curr Biol* **22**, R966-980.

Lawrence, K. S., Chau, T. and Engebrecht, J. (2015). DNA damage response and spindle assembly checkpoint function throughout the cell cycle to ensure genomic integrity. *PLoS genetics* **11**, e1005150.

Li, M., Li, S., Yuan, J., Wang, Z. B., Sun, S. C., Schatten, H. and Sun, Q. Y. (2009). Bub3 is a spindle assembly checkpoint protein regulating chromosome segregation during mouse oocyte meiosis. *PLoS One* **4**, e7701.

Madgwick, S., Hansen, D. V., Levasseur, M., Jackson, P. K. and Jones, K. T. (2006). Mouse Emi2 is required to enter meiosis II by reestablishing cyclin B1 during interkinesis. *The Journal of cell biology* **174**, 791-801.

Maldonado, M. and Kapoor, T. M. (2011). Constitutive Mad1 targeting to kinetochores uncouples checkpoint signalling from chromosome biorientation. *Nat Cell Biol* **13**, 475-482.

Marangos, P., Stevense, M., Niaka, K., Lagoudaki, M., Nabti, I., Jessberger, R. and Carroll, J. (2015). DNA damage-induced metaphase I arrest is mediated by the spindle assembly checkpoint and maternal age. *Nat Commun* **6**, 8706.

Marangos, P., Verschuren, E. W., Chen, R., Jackson, P. K. and Carroll, J. (2007). Prophase I arrest and progression to metaphase I in mouse oocytes are controlled by Emi1-dependent regulation of APC(Cdh1). *The Journal of cell biology* **176**, 65-75.

Maresca, T. J. and Salmon, E. D. (2009). Intrakinetochore stretch is associated with changes in kinetochore phosphorylation and spindle assembly checkpoint activity. *The Journal of cell biology* **184**, 373-381.

Matson, D. R. and Stukenberg, P. T. (2014). CENP-I and Aurora B act as a molecular switch that ties RZZ/Mad1 recruitment to kinetochore attachment status. *The Journal of cell biology* **205**, 541-554.

Miyanari, Y., Ziegler-Birling, C. and Torres-Padilla, M. E. (2013). Live visualization of chromatin dynamics with fluorescent TALEs. *Nat Struct Mol Biol* **20**, 1321-1324.

Musacchio, A. (2015). The Molecular Biology of Spindle Assembly Checkpoint Signaling Dynamics. *Curr Biol* **25**, R1002-1018.

Nagaoka, S. I., Hassold, T. J. and Hunt, P. A. (2012). Human aneuploidy: mechanisms and new insights into an age-old problem. *Nat Rev Genet* **13**, 493-504.

Nagaoka, S. I., Hodges, C. A., Albertini, D. F. and Hunt, P. A. (2011). Oocyte-specific differences in cell-cycle control create an innate susceptibility to meiotic errors. *Curr Biol* **21**, 651-657.

Nakada, D., Matsumoto, K. and Sugimoto, K. (2003). ATM-related Tel1 associates with double-strand breaks through an Xrs2-dependent mechanism. *Genes Dev* **17**, 1957-1962.

Nguyen, A. L., Gentilello, A. S., Balboula, A. Z., Shrivastava, V., Ohring, J. and Schindler, K. (2014). Phosphorylation of threonine 3 on histone H3 by haspin kinase is required for meiosis I in mouse oocytes. *J Cell Sci* **127**, 5066-5078.

Niault, T., Hached, K., Sotillo, R., Sorger, P. K., Maro, B., Benezra, R. and Wassmann, K. (2007). Changing Mad2 levels affects chromosome segregation and spindle assembly checkpoint control in female mouse meiosis I. *PLoS One* **2**, e1165.

Orthwein, A., Fradet-Turcotte, A., Noordermeer, S. M., Canny, M. D., Brun, C. M., Strecker, J., Escribano-Diaz, C. and Durocher, D. (2014). Mitosis inhibits DNA double-strand break repair to guard against telomere fusions. *Science* **344**, 189-193.

Quartuccio, S. M., Dipali, S. S. and Schindler, K. (2017). Haspin inhibition reveals functional differences of interchromatid axis-localized AURKB and AURKC. *Mol Biol Cell*.

Rattani, A., Wolna, M., Ploquin, M., Helmhart, W., Morrone, S., Mayer, B., Godwin, J., Xu, W., Stemmann, O., Pendas, A., et al. (2013). Sgol2 provides a regulatory platform that coordinates essential cell cycle processes during meiosis I in oocytes. *Elife* **2**, e01133.

Ruzankina, Y., Schoppy, D. W., Asare, A., Clark, C. E., Vonderheide, R. H. and Brown, E. J. (2009). Tissue regenerative delays and synthetic lethality in adult mice after combined deletion of Atr and Trp53. *Nat Genet* **41**, 1144-1149.

Salmon, E. D. and Segall, R. R. (1980). Calcium-labile mitotic spindles isolated from sea urchin eggs (Lytechinus variegatus). *The Journal of cell biology* **86**, 355-365.

Santaguida, S., Vernieri, C., Villa, F., Ciliberto, A. and Musacchio, A. (2011). Evidence that Aurora B is implicated in spindle checkpoint signalling independently of error correction. *EMBO J* **30**, 1508-1519.

Schindler, K., Davydenko, O., Fram, B., Lampson, M. A. and Schultz, R. M. (2012). Maternally recruited Aurora C kinase is more stable than Aurora B to support mouse oocyte maturation and early development. *Proc Natl Acad Sci U S A* **109**, E2215-2222.

Schweizer, N., Ferras, C., Kern, D. M., Logarinho, E., Cheeseman, I. M. and Maiato, H. (2013). Spindle assembly checkpoint robustness requires Tpr-mediated regulation of Mad1/Mad2 proteostasis. *The Journal of cell biology* **203**, 883-893.

Sebestova, J., Danylevska, A., Novakova, L., Kubelka, M. and Anger, M. (2012). Lack of response to unaligned chromosomes in mammalian female gametes. *Cell Cycle* **11**, 3011-3018.

Sharif, B., Na, J., Lykke-Hartmann, K., McLaughlin, S. H., Laue, E., Glover, D. M. and Zernicka-Goetz, M. (2010). The chromosome passenger complex is required for fidelity of chromosome transmission and cytokinesis in meiosis of mouse oocytes. *J Cell Sci* **123**, 4292-4300.

Shuda, K., Schindler, K., Ma, J., Schultz, R. M. and Donovan, P. J. (2009). Aurora kinase B modulates chromosome alignment in mouse oocytes. *Mol Reprod Dev* **76**, 1094-1105.

Sirbu, B. M. and Cortez, D. (2013). DNA damage response: three levels of DNA repair regulation. *Cold Spring Harb Perspect Biol* **5**, a012724.

Terasawa, M., Shinohara, A. and Shinohara, M. (2014). Canonical non-homologous end joining in mitosis induces genome instability and is suppressed by M-phase-specific phosphorylation of XRCC4. *PLoS genetics* **10**, e1004563.

Thanisch, K., Schneider, K., Morbitzer, R., Solovei, I., Lahaye, T., Bultmann, S. and Leonhardt, H. (2014). Targeting and tracing of specific DNA sequences with dTALEs in living cells. *Nucleic Acids Res* **42**, e38.

Toso, A., Winter, J. R., Garrod, A. J., Amaro, A. C., Meraldi, P. and McAinsh, A. D. (2009). Kinetochore-generated pushing forces separate centrosomes during bipolar spindle assembly. *The Journal of cell biology* **184**, 365-372.

Touati, S. A., Buffin, E., Cladiere, D., Hached, K., Rachez, C., van Deursen, J. M. and Wassmann, K. (2015). Mouse oocytes depend on BubR1 for proper chromosome segregation but not for prophase I arrest. *Nat Commun* **6**, 6946.

Touati, S. A. and Wassmann, K. (2016). How oocytes try to get it right: spindle checkpoint control in meiosis. *Chromosoma* **125**, 321-335.

Tsurumi, C., Hoffmann, S., Geley, S., Graeser, R. and Polanski, Z. (2004). The spindle assembly checkpoint is not essential for CSF arrest of mouse oocytes. *The Journal of cell biology* **167**, 1037-1050.

Uchida, K. S., Takagaki, K., Kumada, K., Hirayama, Y., Noda, T. and Hirota, T. (2009). Kinetochore stretching inactivates the spindle assembly checkpoint. *The Journal of cell biology* **184**, 383-390.

Wang, F., Dai, J., Daum, J. R., Niedzialkowska, E., Banerjee, B., Stukenberg, P. T., Gorbsky, G. J. and Higgins, J. M. (2010). Histone H3 Thr-3 phosphorylation by Haspin positions Aurora B at centromeres in mitosis. *Science* **330**, 231-235.

Wang, F., Ulyanova, N. P., Daum, J. R., Patnaik, D., Kateneva, A. V., Gorbsky, G. J. and Higgins, J. M. (2012). Haspin inhibitors reveal centromeric functions of Aurora B in chromosome segregation. *The Journal of cell biology* **199**, 251-268.

Wang, Q., Wei, H., Du, J., Cao, Y., Zhang, N., Liu, X., Liu, X., Chen, D. and Ma, W. (2016). H3 Thr3 phosphorylation is crucial for meiotic resumption and anaphase onset in oocyte meiosis. *Cell Cycle* **15**, 213-224.

Waters, J. C., Chen, R. H., Murray, A. W. and Salmon, E. D. (1998). Localization of Mad2 to kinetochores depends on microtubule attachment, not tension. *The Journal of cell biology* **141**, 1181-1191.

Wu, J. Q. and Kornbluth, S. (2008). Across the meiotic divide - CSF activity in the post-Emi2/XErp1 era. *J Cell Sci* **121**, 3509-3514.

Yang, C., Hao, J., Kong, D., Cui, X., Zhang, W., Wang, H., Guo, X., Ma, S., Liu, X., Pu, P., et al. (2014). ATM-mediated Mad1 Serine 214 phosphorylation regulates Mad1 dimerization and the spindle assembly checkpoint. *Carcinogenesis* **35**, 2007-2013.

Yun, Y., Lane, S. I. and Jones, K. T. (2014). Premature dyad separation in meiosis II is the major segregation error with maternal age in mouse oocytes. *Development* **141**, 199-208.

Zhang, D., Li, M., Ma, W., Hou, Y., Li, Y. H., Li, S. W., Sun, Q. Y. and Wang, W. H. (2005). Localization of mitotic arrest deficient 1 (MAD1) in mouse oocytes during the first meiosis and its functions as a spindle checkpoint protein. *Biol Reprod* **72**, 58-68.

Zhang, T., Zhou, Y., Wang, H. H., Meng, T. G., Guo, L., Ma, X. S., Shen, W., Schatten, H. and Sun, Q. Y. (2016). Spc24 is required for meiotic kinetochore-microtubule attachment and production of euploid eggs. *Oncotarget* **7**, 71987-71997.

Zhou, H., Wang, T., Zheng, T., Teng, J. and Chen, J. (2016). Cep57 is a Mis12-interacting kinetochore protein involved in kinetochore targeting of Mad1-Mad2. *Nat Commun* **7**, 10151.

Figure Legends

Figure 1. DNA damage rapidly inactivates the APC during meiosis I in mouse oocytes. (**A**) Degradation of securin-YFP fluorescence per unit time (%h^{-1}) relative to the time of DMSO, etoposide or nocodazole. *, indicates statistical difference compared to time of drug addition ($P < 0.05$, ANOVA with Dunnett's multiple comparison test). (**B**) Mean time from drug addition to stabilization (i.e. net loss of fluorescence is zero) of securin-YFP, from data shown in (a). Oocytes expressing securin-YFP were matured to 6 h after NEB. Error bars indicate s.d.

Figure 2. Recruitment of Mad1 to bivalents following DNA damage. (**A**) Representative images in oocytes expressing Mad1-2GFP and H2B-mCherry, tracked in MI by responsive time-lapse. (**B**) Quantification of bivalent-associated Mad1 signal recorded in (a). (**C,D,E,F)** Representative images (C,E) and quantification (D,F) of Mad1 signal on bivalents following addition of either nocodazole (C,D) or etoposide (E,F). Images captured at 5 min timepoints 6 h after NEB. (B,D,F) normalised to the maximum signal. A,C,E, Scale bars represent 10 µm. (D,F) *, indicates significant difference from 0 min ($P<0.0001$, ANOVA with Tukey's multiple comparisons test).

Figure 3. Recruitment of Mad1 following DNA damage requires Mps1 and Aurora kinase activity. (A,B) Bivalents from oocytes expressing Mad1-GFP and H2B-mCherry were tracked in MI by responsive time-lapse and images recorded every 5 min. Representative images showing Mad1 and H2B with etoposide addition, followed by either AZ3146 (A) or ZM447439 (B). The Mad1 signal is quantified above the corresponding images, normalised to the maximum signal. Scale bars, 10 µm.

Figure 4. Haspin kinase inhibition prevents Mad1 kinetochore recruitment following DNA damage. (A) Representative images of oocytes 6 h after NEB expressing Mad1-GFP and H2B-mCherry. Addition of vehicle control (0.1% ethanol) or haspin kinase inhibitor (5-Iodotubercidin, 0.1%) occurred prior to imaging. Both groups were also treated with 10 µM MG132 to prevent entry into anaphase. Etoposide was added at time 0. Scale bars,

10 µm. (**B**) Quantification of the Mad1 signal from oocytes in A. Individual traces in pale colours and means in bold. * indicate significant differences (P<0.003, t-test).

Figure 5. SAC proteins form discrete foci at centromeres following DNA damage. (A,B,C,D) Mad1-GFP (A,C) or Cdc20-GFP (B,D) fluorescence in oocytes co-expressing H2B-mCherry 1 h after addition of etoposide (A,B) or nocodazole (C,D). Insets show a representative bivalent, whose Mad1 or Cdc20 intensity is plotted along the axial length of the bivalent. Background readings were taken from a nearby area containing no chromosomes. For all plots Mad1 and Cdc20 fluorescence is only located in the centromeric region of the mouse telocentric bivalents. Scale bar, 5 µm.

Figure 6. DNA damage does not reduce kinetochore-microtubule attachment or tension. (A) K-fibres immunostained for tubulin and anti-centromere antigen (ACA; counterstained with DAPI). Two bivalents are enlarged, showing examples of attached (arrows) and unattached (arrowhead) kinetochores. (**B**) Frequency of kinetochore attachment to k-fibres following etoposide, nocodazole, or vehicle (0.1% DMSO). Number of kinetochores assessed are shown in parenthesis. Statistical test was Fisher's exact, error bars represent 95% confidence intervals. (**C**) Bivalents in an oocyte expressing Spc24-mCherry, a TALE protein against the major satellite repeat (Maj. Sat.-mClover), and counterstained with Hoechst; at 7 h after NEB. Inset (white corner square) and cartoon show the measurements made on each bivalent: inter-homolog kinetochore stretch (ihK-K), and centromere-kinetochore stretch (C-K). (**D,E**) Measures of ihK-K (d) and C-K (E) following treatment with vehicle (DMSO, 0.1%), etoposide or monastrol (100 µM). Error bars indicate s.d; number of measurements are in parenthesis, different letters indicate statistically significant differences (P<0.05, ANOVA with Tukey's multiple comparison test).

Figure 7. Meiotic DNA damage induced SAC activation is independent of ATM and ATR kinases. (A) Representative γH2AX staining in the nuclei of

oocytes before NEB, following addition of etoposide, or etoposide with ATMi (KU55933) and ATRi (ATR kinase inhibitor II). Scale bar, 5 μm. (**B**) Quantification of γH2AX levels from (A). Number of oocytes in parenthesis. Different letters indicate significant difference (P<0.0001, ANOVA with Dunn's multiple comparison test). (**C**) Percentage of oocytes completing MI following treatment with either etoposide or DMSO vehicle before NEB. Groups were matured in the presence or absence of ATMi and ATRi, and scored for polar body extrusion. (**D**) Oocytes from mice that were conditional double knockouts for ATR and ATM, or floxed littermate controls were exposed to etoposide or a vehicle control, and assessed for completion of MI. (C,D) Number of oocytes used indicated in parenthesis, statistical test used was Fisher's exact (ns, not significant).

Figure 8. DNA damaged mature eggs can complete meiosis II. (A,B) Representative timelapse of Mad1-GFP recruitment to the chromosomes of a meiosis I oocyte (A) and metII egg (B), following etoposide and nocodazole addition. Oocytes co-express H2B-mcherry. (**C**) Quantification of kinetochore associated Mad1 after etoposide addition to oocytes or eggs. Fluorescence was normalised for each cell with respect to its maximal value following nocodazole addition. Error bars indicate s.d. Different letters indicate statistically different groups (P<0.0001, ANOVA with Tukey's multiple comparison test). (**D**) Parthenogenetic egg activation rates following either etoposide or nocodazole addition as indicated. Number of oocytes used indicated in parenthesis; different letters indicate statistically different groups (P<0.005, Fisher's exact test with Bonferroni correction for multiple comparisons).

Figure 9. Model to explain meiosis I specific SAC arrest following DNA damage. Possible mechanisms by which the SAC/DDR checkpoint functions specifically in meiosis I. (**A**) A meiosis I specific protein may transduce a signal from sites of DNA damage in close proximity to the kinetochore to allow SAC signalling on the kinetochore, alternatively, this may happen due to the unique proximity of the two sister kinetochores in meiosis I. (**B**) the large

volume of chromatin under tension during meiosis I may make the bivalent more sensitive to DNA damage when compared to meiosis II or to mitosis.

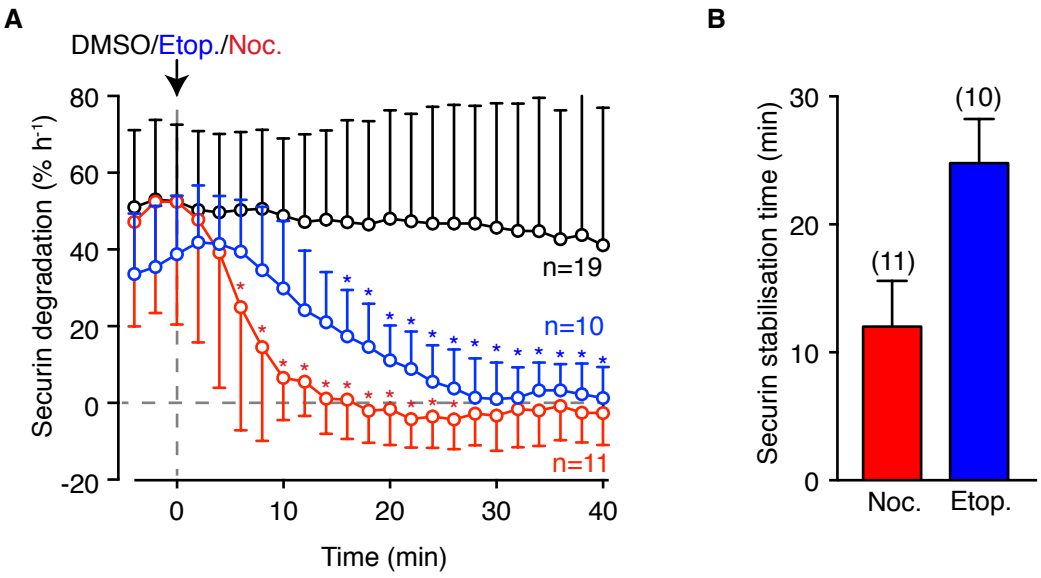
A
DMSO/Etop./Noc.
Securin degradation (% h-1)
80
60
40
20
0
-20
0
10
20
30
40
Time (min)
n=19
n=10
n=11
B
Securin stabilisation time (min)
30
20
10
0
(11)
(10)
Noc.
Etop.

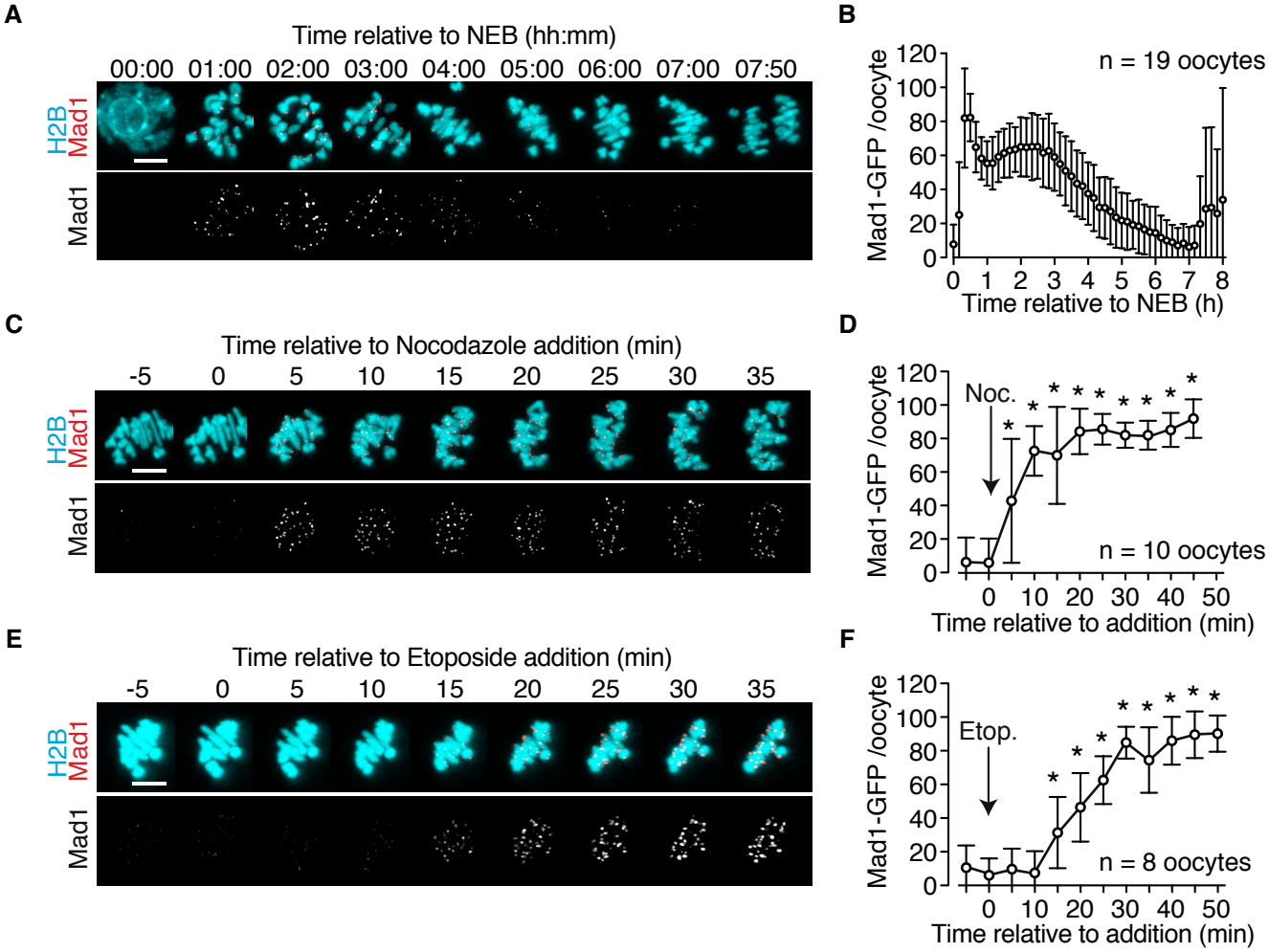
A
Time relative to NEB (hh:mm)
00:00 01:00 02:00 03:00 04:00 05:00 06:00 07:00 07:50
H2B Mad1
Mad1
B
n = 19 oocytes
Mad1-GFP /oocyte
Time relative to NEB (h)
C
Time relative to Nocodazole addition (min)
-5 0 5 10 15 20 25 30 35
H2B Mad1
Mad1
D
Noc.
n = 10 oocytes
Mad1-GFP /oocyte
Time relative to addition (min)
E
Time relative to Etoposide addition (min)
-5 0 5 10 15 20 25 30 35
H2B Mad1
Mad1
F
Etop.
n = 8 oocytes
Mad1-GFP /oocyte
Time relative to addition (min)

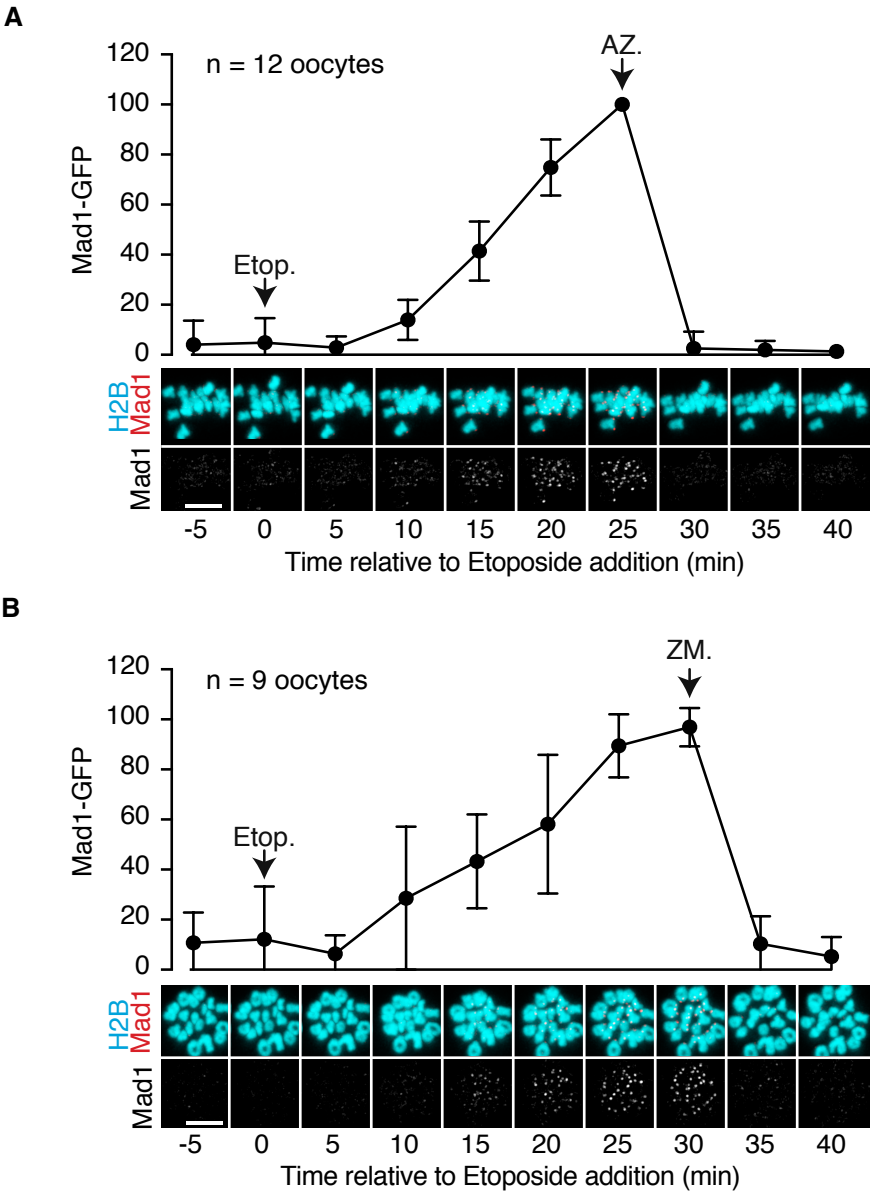
A
n = 12 oocytes
AZ.
Etop.
Mad1-GFP
120
100
80
60
40
20
0
H2B Mad1
Mad1
-5
0
5
10
15
20
25
30
35
40
Time relative to Etoposide addition (min)
B
n = 9 oocytes
ZM.
Etop.
Mad1-GFP
120
100
80
60
40
20
0
H2B Mad1
Mad1
-5
0
5
10
15
20
25
30
35
40
Time relative to Etoposide addition (min)

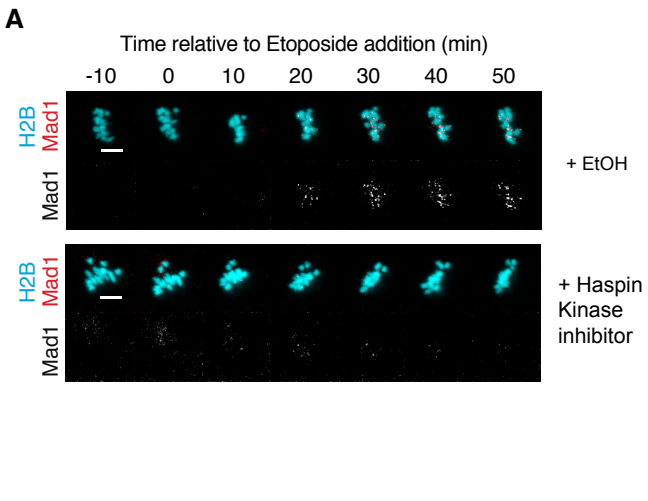
A
Time relative to Etoposide addition (min)
-10
0
10
20
30
40
50
H2B
Mad1
Mad1
+ EtOH
H2B
Mad1
Mad1
+ Haspin
Kinase
inhibitor

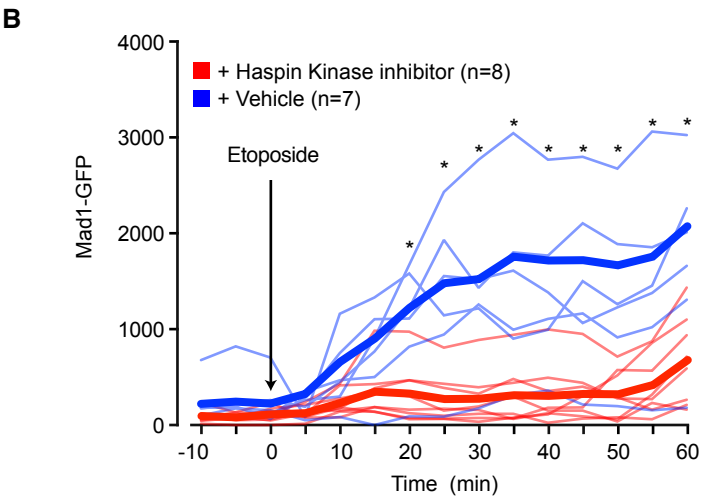
B
4000
3000
2000
1000
0
Mad1-GFP
+ Haspin Kinase inhibitor (n=8)
+ Vehicle (n=7)
Etoposide
-10
0
10
20
30
40
50
60
Time (min)

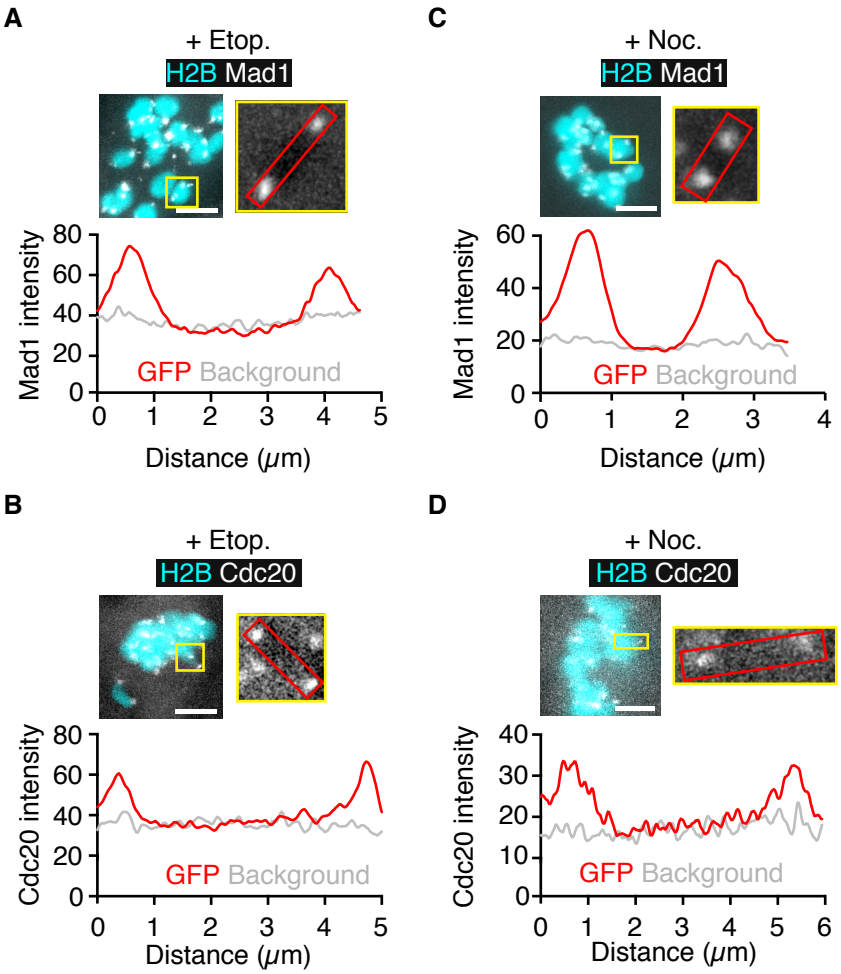
A
+ Etop.
H2B Mad1
Mad1 intensity
GFP Background
Distance (μm)
C
+ Noc.
H2B Mad1
Mad1 intensity
GFP Background
Distance (μm)
B
+ Etop.
H2B Cdc20
Cdc20 intensity
GFP Background
Distance (μm)
D
+ Noc.
H2B Cdc20
Cdc20 intensity
GFP Background
Distance (μm)

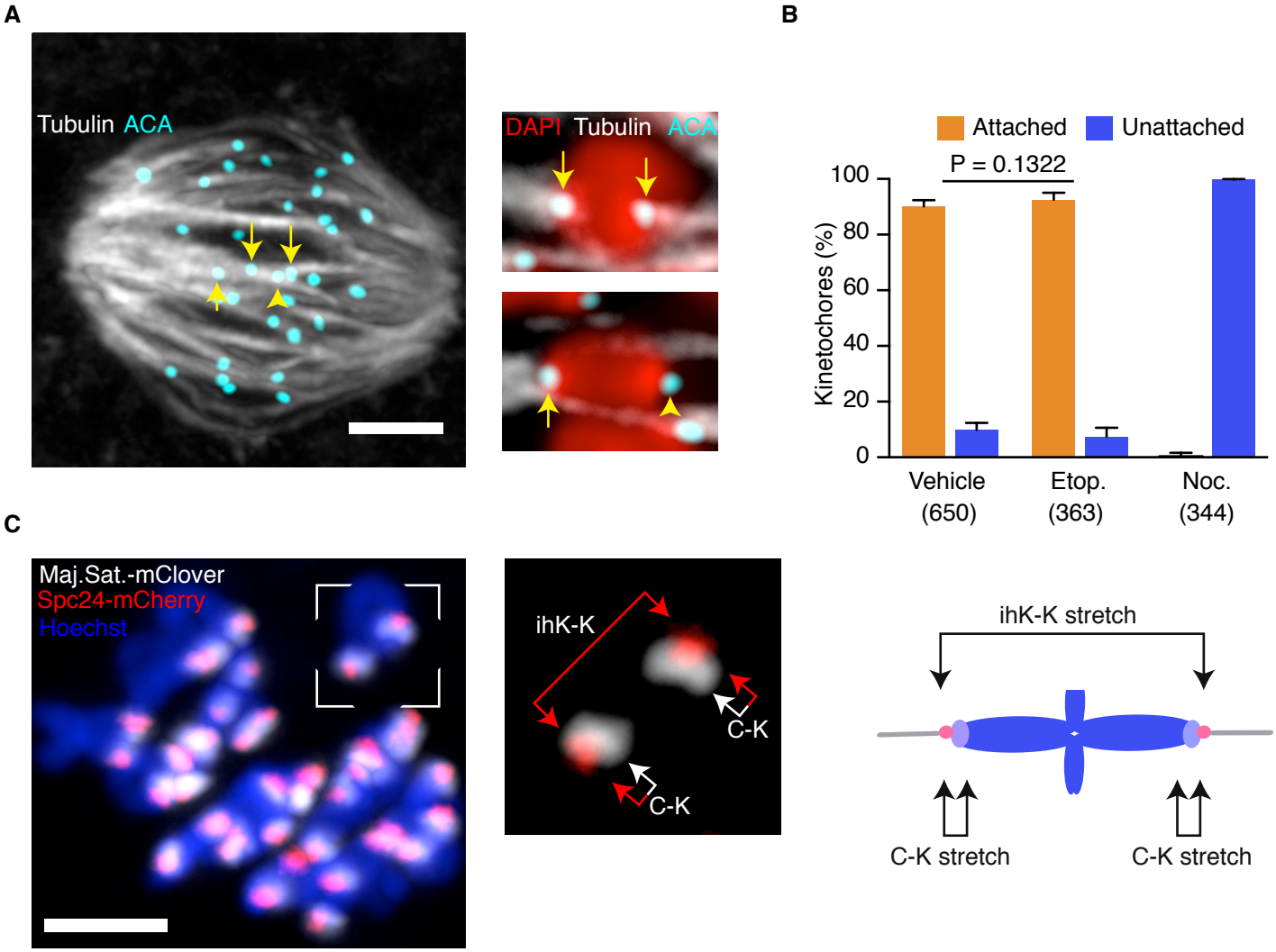
A
Tubulin ACA
DAPI Tubulin ACA
B
Attached
Unattached
P = 0.1322
Kinetochores (%)
100
80
60
40
20
0
Vehicle
(650)
Etop.
(363)
Noc.
(344)
C
Maj.Sat.-mClover
Spc24-mCherry
Hoechst
ihK-K
C-K
C-K
ihK-K stretch
C-K stretch
C-K stretch
D
ihK-K (μm)
10
8
6
4
2
0
A
(119)
A
(113)
B
(65)
Vehicle
Etop.
Mon.
E
C-K (μm)
1.5
1.0
0.5
0.0
A
(238)
A
(226)
B
(130)
Vehicle
Etop.
Mon.

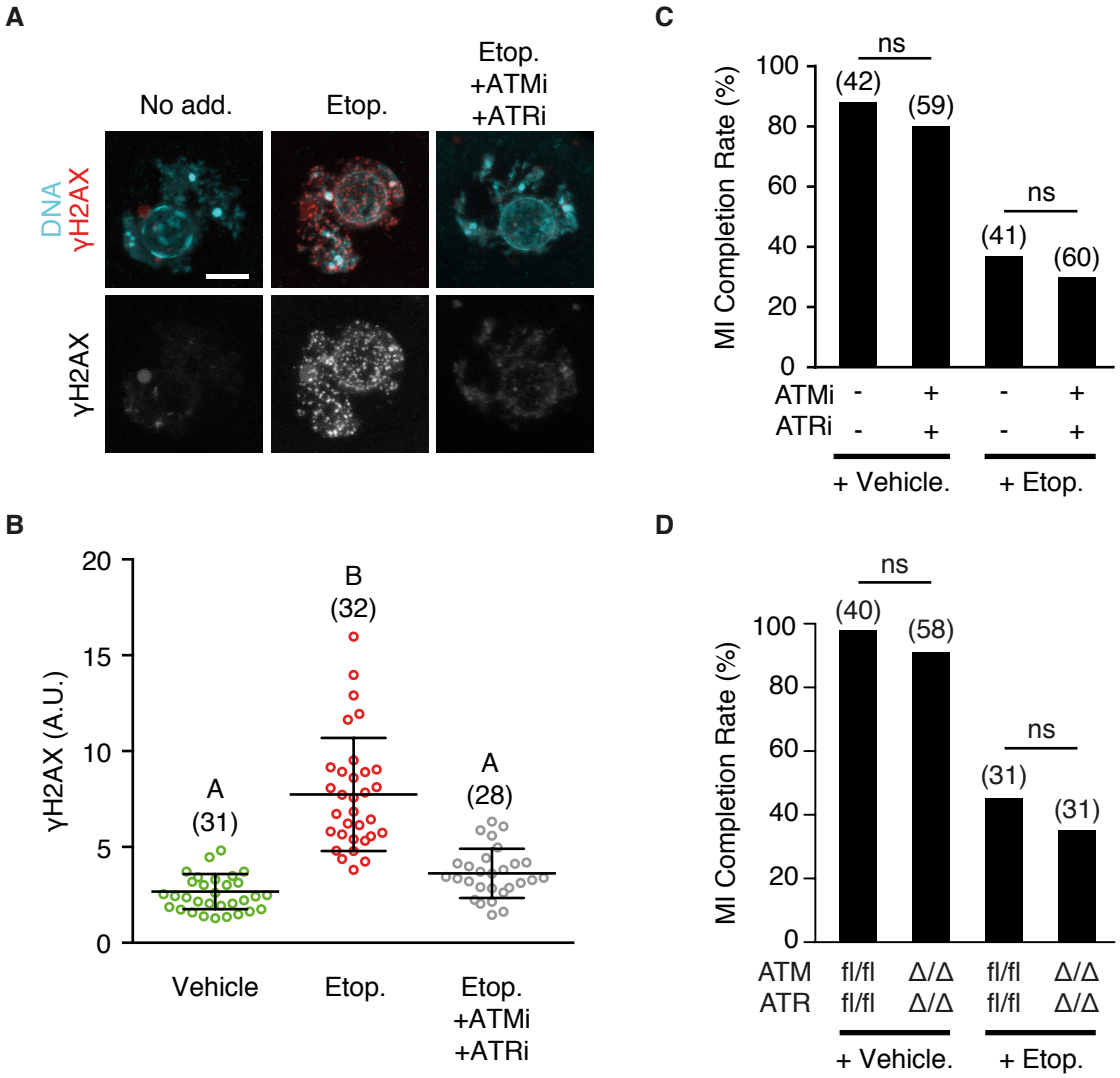
A
No add.
Etop.
Etop.
+ATMi
+ATRi
DNA
γH2AX
γH2AX
B
γH2AX (A.U.)
20
15
10
5
0
A
(31)
B
(32)
A
(28)
Vehicle
Etop.
Etop.
+ATMi
+ATRi
C
MI Completion Rate (%)
100
80
60
40
20
0
ns
(42)
(59)
ns
(41)
(60)
ATMi - + - +
ATRi - + - +
+ Vehicle.
+ Etop.
D
MI Completion Rate (%)
100
80
60
40
20
0
ns
(40)
(58)
ns
(31)
(31)
ATM fl/fl Δ/Δ fl/fl Δ/Δ
ATR fl/fl Δ/Δ fl/fl Δ/Δ
+ Vehicle.
+ Etop.

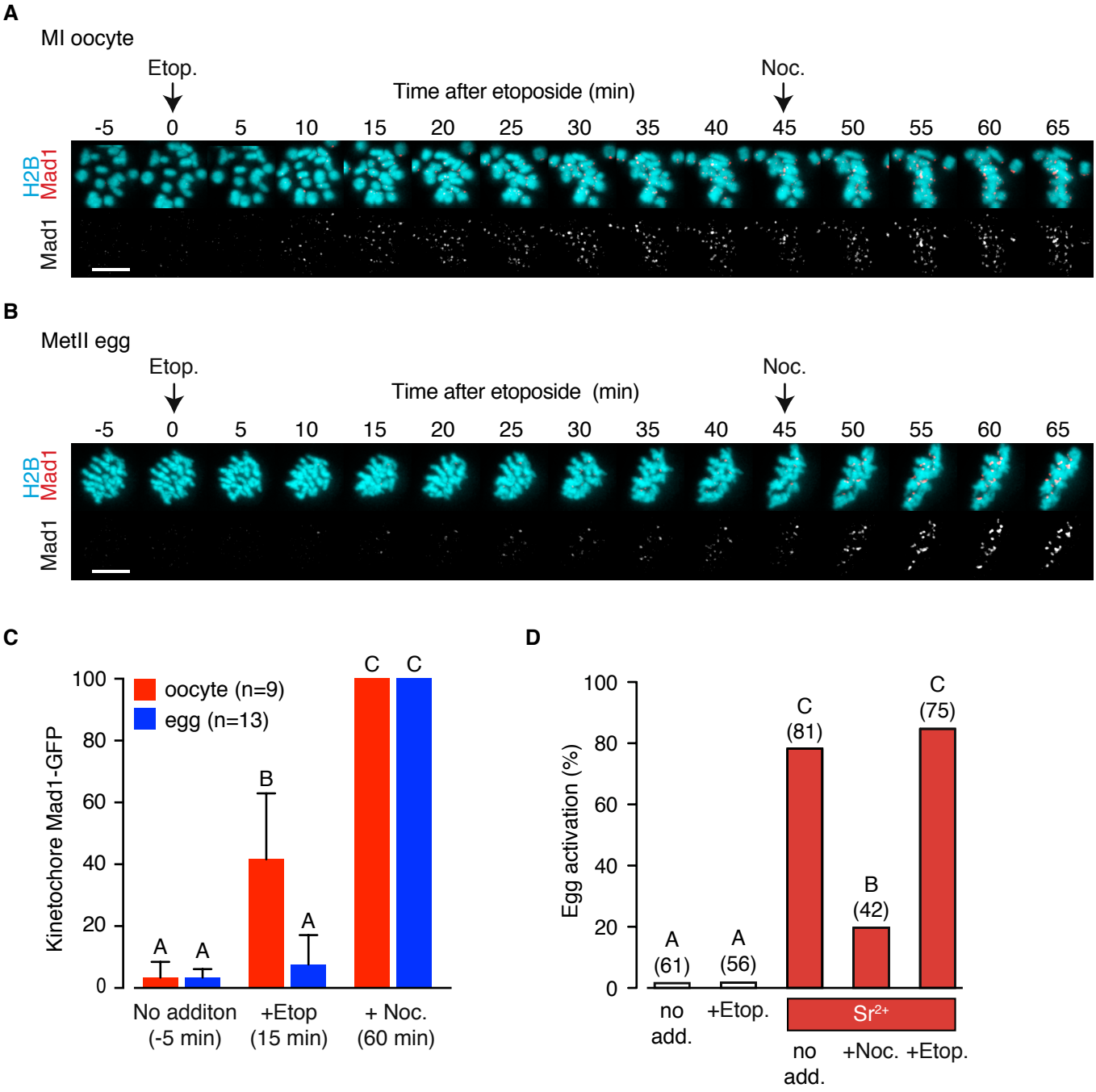
A
MI oocyte
Etop.
Noc.
Time after etoposide (min)
-5 0 5 10 15 20 25 30 35 40 45 50 55 60 65
H2B Mad1
Mad1
B
MetII egg
Etop.
Noc.
Time after etoposide (min)
-5 0 5 10 15 20 25 30 35 40 45 50 55 60 65
H2B Mad1
Mad1
C
Kinetochore Mad1-GFP
100 80 60 40 20 0
oocyte (n=9)
egg (n=13)
A A B A C C
No additon (-5 min)
+Etop (15 min)
+ Noc. (60 min)
D
Egg activation (%)
100 80 60 40 20 0
A (61)
A (56)
C (81)
B (42)
C (75)
no add.
+Etop.
Sr2+
no add.
+Noc.
+Etop.

A

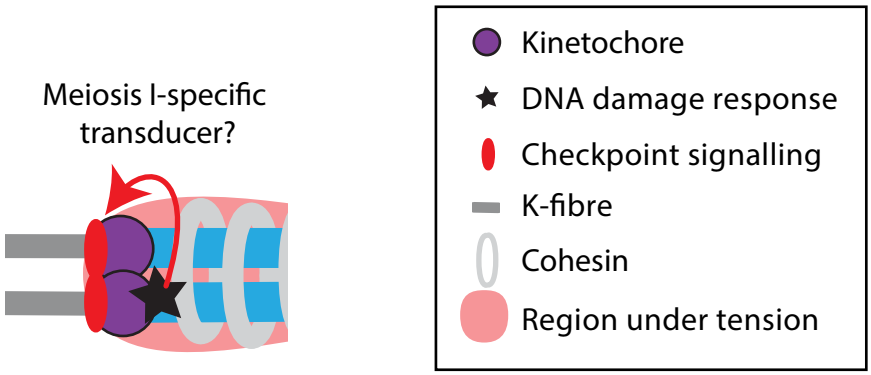
Meiosis I-specific transducer?
Kinetochore
DNA damage response
Checkpoint signalling
K-fibre
Cohesin
Region under tension

B

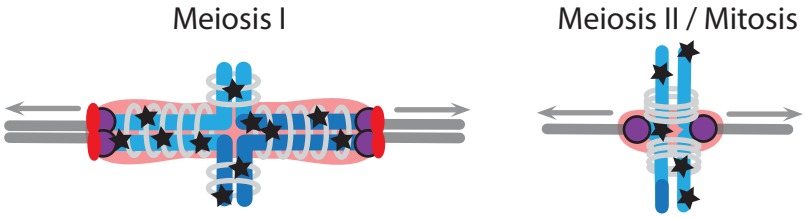
Meiosis I
Meiosis II / Mitosis

Supplementary Figures

Figure S1. Mad1 can be rapidly moved on or off kinetochores in meiosis I using nocodazole or reversine. (**A**) Representative images of metaphase I oocytes expressing Mad1-GFP and H2B-mCherry. Addition of nocodazole (Noc.), but not vehicle control (DMSO) caused a rapid (5-10 min) increase in chromosome associated Mad1. (**B**) Data from images as in 'A'. (**C**) Following addition of nocodazole, reversine (Rev.) could rapidly cause loss of Mad1-GFP from kinetochores (5 min). (**D**) Data from images as in 'C'. **A-D** Arrows indicate time of drug addition. **A,C** Scale bars, 10 μm. **B,D** Error bars, indicate s.d.

A

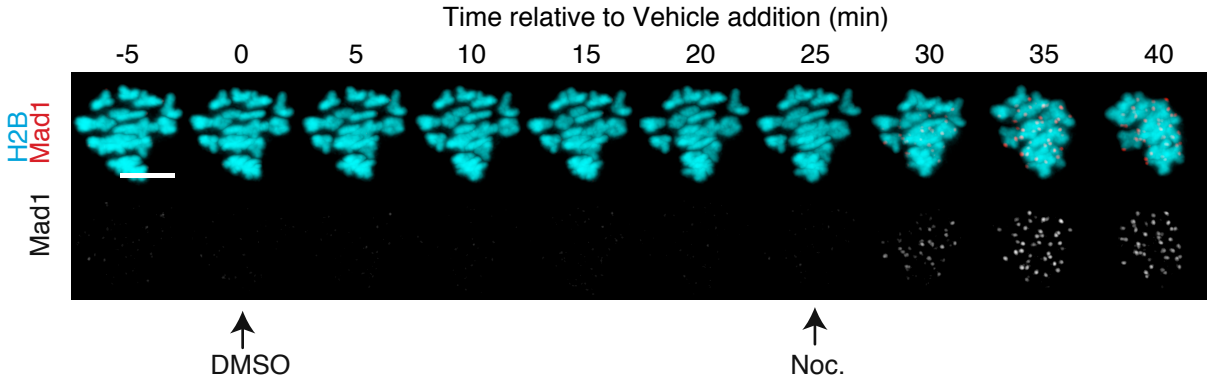
Time relative to Vehicle addition (min)
-5
0
5
10
15
20
25
30
35
40
H2B
Mad1
Mad1
DMSO
Noc.

B

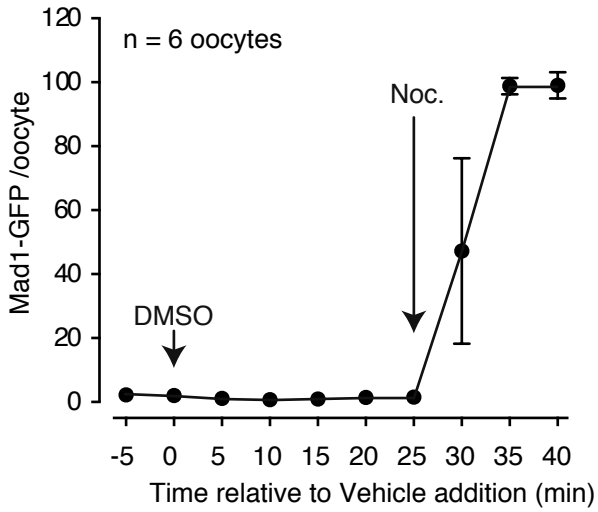
n = 6 oocytes
Noc.
DMSO
Mad1-GFP /oocyte
120
100
80
60
40
20
0
-5
0
5
10
15
20
25
30
35
40
Time relative to Vehicle addition (min)

C

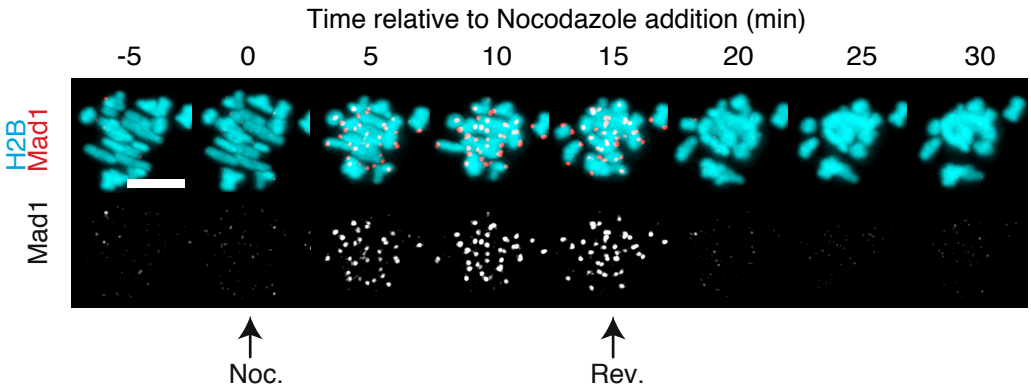
Time relative to Nocodazole addition (min)
-5
0
5
10
15
20
25
30
H2B
Mad1
Mad1
Noc.
Rev.

D

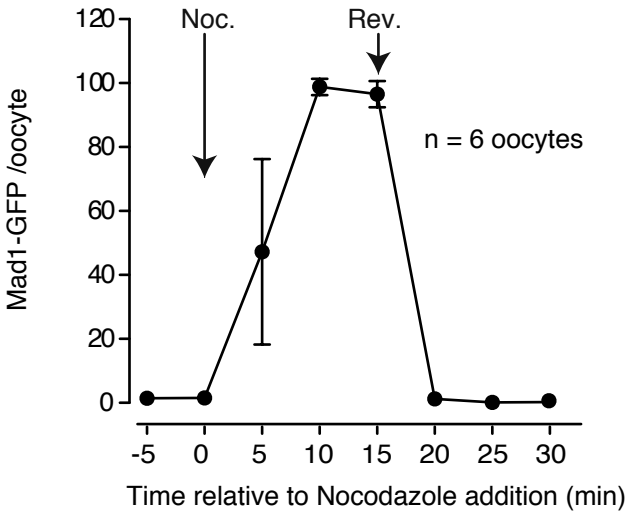
Noc.
Rev.
n = 6 oocytes
Mad1-GFP /oocyte
120
100
80
60
40
20
0
-5
0
5
10
15
20
25
30
Time relative to Nocodazole addition (min)

Figure S2. Extensive DNA damage does not recruit Mad1 to chromosome arms. (**A**) Representative (n=18) z-projection images of oocytes expressing Mad1-GFP (Red/Grey) and H2B-mCherry (Cyan) following 15 min of treatment with 400 μM etoposide (10x that used elsewhere). Scale bar, 10 μm. Area in white box is enlarged below and shows a single z-slice. (**B**) Intensity plot of Mad1-GFP and H2B-mCherry along the long axis of the bivalent as well as a background Mad1-GFP signal taken from a nearby region with no chromosomes.

A

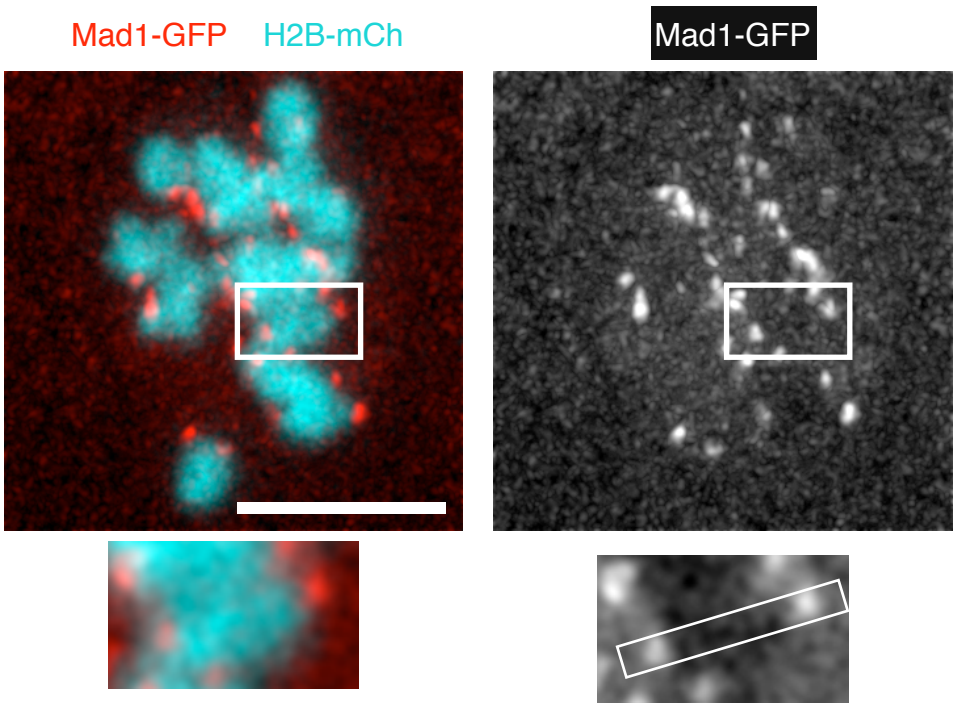
Mad1-GFP H2B-mCh
Mad1-GFP

B

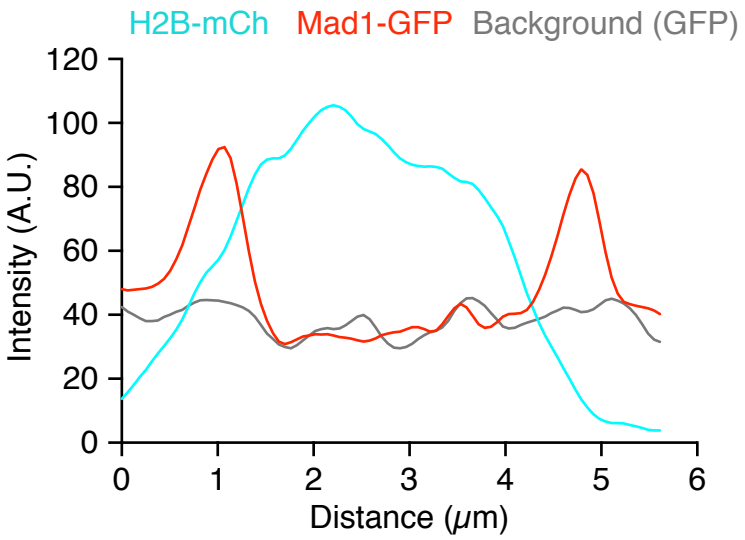
H2B-mCh
Mad1-GFP
Background (GFP)
Intensity (A.U.)
120
100
80
60
40
20
0
0
1
2
3
4
5
6
Distance (μm)

Figure S3. ATM/ATR kinase inhibitors reduce γH2AX foci in GV oocytes. GV oocytes were treated with or without etoposide (15 mins) in the presence or absence of kinase inhibitors for ATM or ATR. (**A**) Representative z-projection images of the oocyte nucleus show Hoechst (cyan) and γH2AX (red). Scale bar, 10 μm. (**B**) Quantification of the nuclear γH2AX signal from images in 'A'. Number of oocytes indicated in parenthesis. Different letters indicate significant difference between groups ($P<0.05$, ANOVA with Tukey's multiple comparison test).

A

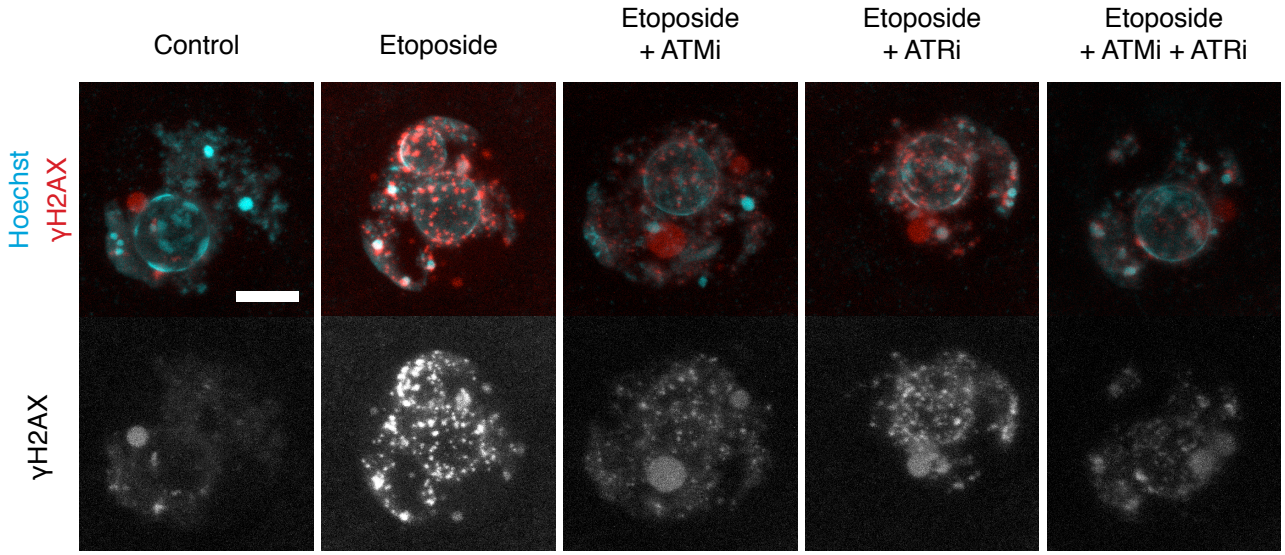
Control
Etoposide
Etoposide + ATMi
Etoposide + ATRi
Etoposide + ATMi + ATRi
Hoechst
γH2AX
γH2AX

B

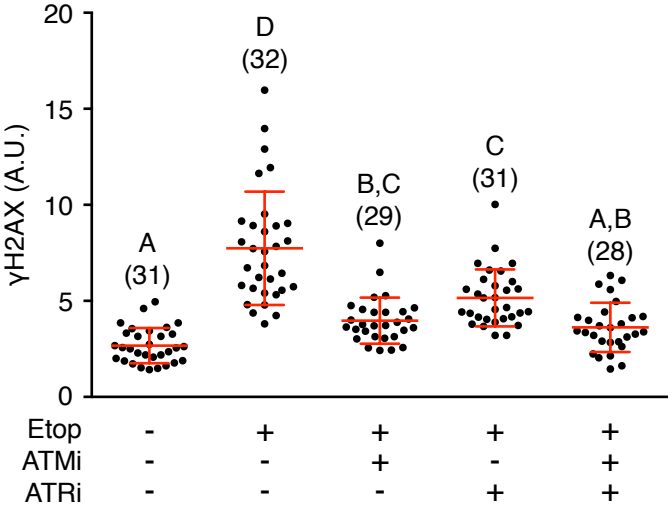
γH2AX (A.U.)
20
15
10
5
0
A (31)
D (32)
B,C (29)
C (31)
A,B (28)
Etop - + + + +
ATMi - - + - +
ATRi - - - + +

Figure S4. MetII eggs do not arrest in response to UV damage. (**A**) GV oocytes were placed on the UV illuminator with or without 300nm irradiation for 30 s and scored for completion of meiosis I 14 h later. P-value calculated by Fisher's exact test. (**B**) MetII eggs were treated with or without UV irradiation as in 'A', and were then either activated by 7% ethanol, or untreated as indicated. Six hours later eggs were scored for activation by observing pronuclear formation. Different letters indicate statistically significant differences ($P<0.001$, Fisher's exact test with Bonferroni correction for multiple comparisons). (A,B) number of oocytes/eggs indicated in parenthesis.

A

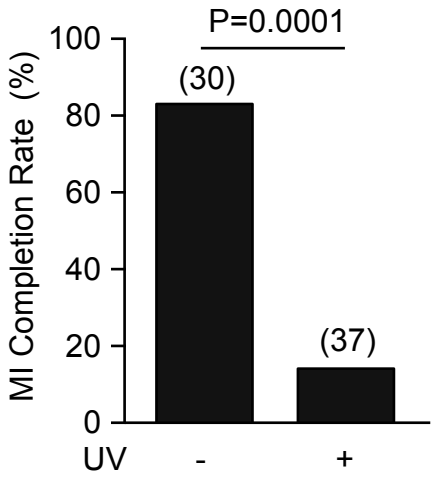
P=0.0001
100
80
60
40
20
0
MI Completion Rate (%)
(30)
(37)
UV
-
+

B

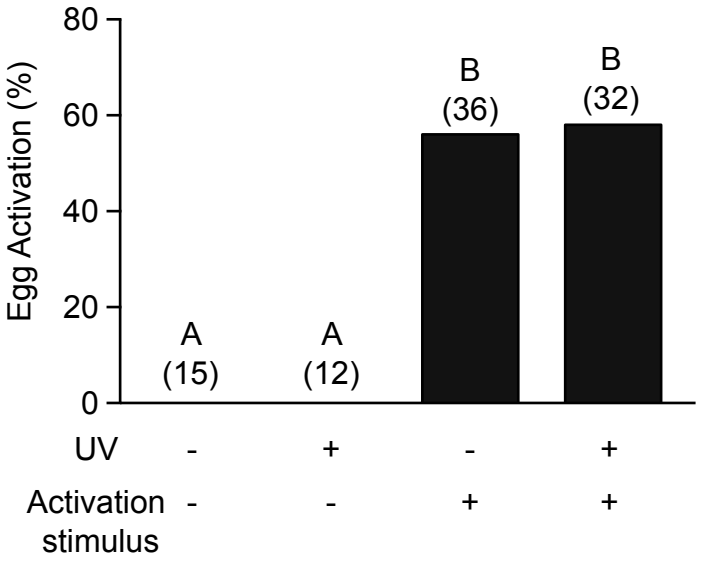
80
60
40
20
0
Egg Activation (%)
A
(15)
A
(12)
B
(36)
B
(32)
UV
-
+
-
+
Activation stimulus
-
-
+
+